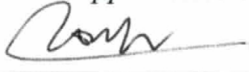


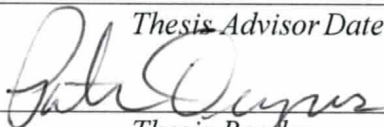
**NORTHEASTERN UNIVERSITY
GRADUATE SCHOOL OF COMPUTER SCIENCE
Ph.D. THESIS APPROVAL FORM**

THESIS TITLE: Wireless Transfer of Energy Alongside Information: From Wireless Sensor Networks to Bio-Enabled Wireless Networks

AUTHOR: Hooman Javaheri

Ph.D. Thesis Approved to complete all degree requirements for the Ph.D. Degree in Computer Science.

 11/30/2012
Thesis Advisor Date

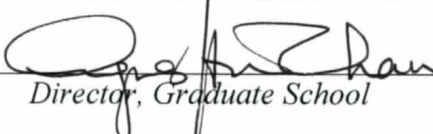
 11/30/2012
Thesis Reader Date

 11/30/12
Thesis Reader Date

 11/30/2012
Thesis Reader Date

D. Starobinski 11/30/2012

GRADUATE SCHOOL APPROVAL:

 12/4/2012
Director, Graduate School Date

COPY RECEIVED IN GRADUATE SCHOOL OFFICE:

Recipient's Signature Date

Distribution: Once completed, this form should be scanned and attached to the front of the electronic dissertation document (page 1). An electronic version of the document can then be uploaded to the Northeastern University-UMI website.

Wireless Transfer of Energy Alongside Information:
From Wireless Sensor Networks to Bio-Enabled
Wireless Networks

A dissertation presented
by

Hooman Javaheri

to the Faculty of Graduate School
of the College of Computer and Information Science
in partial fulfillment of the requirements for the degree of
Doctor of Philosophy

Northeastern University
Boston, MA
November 2012

Abstract

Despite their constant evolution over the last few decades, wireless communication networks still struggle with energy conservation. The problem manifests itself in many applications, in particular wireless sensor networks, where communications do not occur frequently and nodes often remain idle, and also small-scale communication networks, whose nodes need to be minuscule. Such applications can achieve optimal energy-efficiency using passive (battery-less) receivers that wirelessly receive energy and information at the same time. In this thesis, we present techniques to simultaneously deliver energy alongside information during wireless communications.

First, we present mechanisms to consolidate energy and information transfer in wireless sensor networks. We introduce iPoint, a communication system including a passively-powered wireless receiver capable of establishing two-way communication with a commodity smartphone. In contrast to traditional RFID tags, iPoint provides high computation and sensing capabilities and most importantly does not require specialized reader device to communicate. We prototype and experimentally evaluate our design that includes optimization techniques to ensure efficient delivery of energy and information and novel communication protocols.

In the second part of our work, we study energy and information transfer at small scale, particularly in biological systems. We introduce Bio-enabled Wireless Networks (BWN); these theoretical networks feature wireless communication between wireless nodes and tiny biological organisms. We introduce possible designs for such networks using several enabling technologies, and present theoretical results on the performance of energy and information transfer. In particular, we conduct a theoretical analysis to investigate the efficiency of wireless energy transfer to an electromagnetically-coupled nanoresonator, a potential building block for future BWNs.

Acknowledgments

First, I would like to express my sincere gratitude to Prof. Guevara Noubir, my adviser. This entire process would have been impossible without his support and guidance throughout my years in CCIS. I am grateful for his ideas, encouragements, and flexibility.

I would also like to thank Dr. Bernardo Barbiellini for sharing his invaluable insight and joyful discussions we had about this work.

I thank my committee members, Prof. Masette Vona, Prof. Peter Desnoyers, and Prof. David Starobinski for their support and feedback that helped me during the preparation of this work. I would also like to thank Prof. Erik-Oliver Blass for helping me improve my thesis proposal, dissertation and final presentation.

I also thank all members, students and professors, of Northeastern's Networking Lab for making these years such memorable ones.

Going through Ph.D. years would have not been possible if not for unconditional love that I have received from my family and great friends, especially my mom, dad and little brother Hiwa whom I have not seen since I arrived in the states, and miss dearly. I am thankful to all my friends¹ in Boston for making this beautiful city my second home, and all the memories that I will cherish for the rest of my life. Finally, a special thanks to my beautiful Ghazal for being there and keeping me going with her constant encouragement and kindness.

¹Emrah deserves a special mention for sharing house, craziness and all those random discussions and shenanigans.

Contents

Contents	VIII
List of Figures	XIII
1 Introduction	1
1.1 Thesis Overview	4
1.2 Dissertation Organization	5
2 CEICh in Wireless Sensor Networks	8
2.1 Overview of CEICh	8
2.2 Design of CEICh	9
2.2.1 Energy Transfer Mechanisms	10
2.2.1.1 Electrodynamic Induction	10
2.2.1.2 Electromagnetic Radiation	10
2.2.2 Energy Transfer Efficiency	11
2.2.3 Signal Amplification	13
2.2.4 Voltage Rectification	13
2.2.5 Signal Characteristics	15
2.2.6 Communications Schemes	16
3 iPoint	19
3.1 Motivation and Possible Applications	19

3.2	Definition of the System with Respect to CEICh Design	20
3.3	Challenges and Approach	20
3.4	Our Solution	21
3.5	Detailed System Architecture	22
3.5.1	Energy Transfer	22
3.5.2	Computation	24
3.5.3	Display	24
3.6	Multimodal Communications	25
3.6.1	Packet Length Modulation (PLM)	25
3.6.1.1	Encoding	25
3.6.1.2	Decoding	26
3.6.1.3	Data Rate Analysis	26
3.6.1.4	Bit Error Rate of PLM	29
3.6.2	LCD Pattern Coding (LPC)	31
3.6.2.1	Encoding	31
3.6.2.2	Decoding	32
3.6.2.3	LPC Rate Analysis:	33
3.7	Optimization Techniques	33
3.7.1	Antenna	34
3.7.1.1	PCB Dipole Antenna	35
3.7.1.2	Yagi-Uda Antennas	36
3.7.1.3	Planar Inverted-F Antenna	36
3.7.2	Recifier	37
3.7.2.1	Diodes	38
3.7.2.2	Load Impedance	39
3.7.2.3	Rectifier Topology	39
3.7.3	Matching Strategy	41
3.7.4	Low-power Computation	42
3.7.4.1	Power-aware Software	42
3.7.4.2	Underclocking	43
3.8	Prototype	43
3.9	Performance Evaluation	46

3.9.1	Range	46
3.9.2	Rectifier Efficiency	47
3.9.3	Duty Cycle of PLM	47
3.9.4	LCD Contrast Test	48
3.9.5	PLM Decoding Performance	49
3.10	Conclusive Remarks	49
4	Energy and Info. Transfer in BWNs	52
4.1	Basic Concepts	54
4.1.1	Information Flow and Biological Sensitivity	55
4.1.2	Speed	56
4.1.3	Energy	56
4.1.4	Complexity	56
4.2	Approach	57
4.2.1	Systematic Noise	58
4.2.2	Signal Transduction	59
4.3	Enabling Technologies	60
4.3.1	Magnetic Nanoparticles	61
4.3.2	Non-radiative Energy Transfer Mechanisms	62
4.3.3	Energy Harvesting	64
5	Energy Transfer Performance of Electromagnetically-Coupled Mechanical Nanoresonators	66
5.1	Background	66
5.1.1	Coupling Types	67
5.1.2	Our Contribution	67
5.2	Theoretical Model	68
5.3	Energy Analysis	71
5.4	Resonant Scattering Analysis	72
5.5	Applications	74
5.5.1	Replacing Magnetic Coupling in Nanotube Radio	75

5.5.2	A Functional Mechanical Nanoresonator in Biological Setting	76
5.5.3	A Carbon Nanotube based Nanoresonator in Biological Setting	78
5.5.3.1	Design and Optimization	81
5.5.3.2	Discussion	84
5.6	Conclusive Remarks	85
6	Related Work	87
6.1	Passively-powered Wireless Systems	87
6.1.1	Radio Frequency Identification (RFID)	87
6.1.2	WISP	87
6.1.3	Near-Field Communication (NFC)	88
6.1.4	Bokode	88
6.1.5	Microwave Power Transmission	89
6.1.6	Resonant Inductive Coupling	89
6.2	Remote Control of Biological Systems	90
6.2.1	Molecular computing and communication	90
6.2.2	Synthetic Biology	90
6.2.3	Extremophiles	91
7	Conclusion and Future Research Directions	93
	Bibliography	96

List of Figures

2.1	The general schematic of CEICh.	9
2.2	The schematics of envelope detector circuit (a) and the clamp circuit (b).	14
2.3	Schematic of Greinacher voltage doubler.	15
3.1	Conceptual illustration of how iPoint device performs.	21
3.2	Detailed diagram of iPoint.	23
3.3	PLM decoding.	27
3.4	Normalized Rate of PLM for different number of messages. It is shown that the best performance is achieved when $M = 5$	28
3.5	Probability density function of the received sample with PLM modulation	30
3.6	LPC Encoding for a M-segment LCD panel.	32
3.7	LPC decoding. To make decoding faster, the user is asked to align the image of the panel within a virtual box, then the frame is sampled only on the intersections of mask grid-lines (Narrow dashed lines).	33
3.8	The design of the dipole antenna optimized for 2.4 GHz.	35
3.9	The design of the Yagi-Uda antenna array optimized for 2.4 GHz.	37
3.10	The design of the Planar Inverted-F Antenna optimized for 2.4 GHz.	38

3.11 Rectifier efficiency versus Input power for different number of the stages.	40
3.12 The impedance matching in action. The standing wave ratio (SWR) of the rectenna is shown before and after careful matching at active mode load.	43
3.13 Power consumption of MCU for different clock frequencies.	44
3.14 The Prototype of iPoint.	45
3.15 Performance of the energy harvester unit.	47
3.16 Energy-harvester efficiency as a function of input power. The shaded region indicates the operating range of the iPoint. Based on our measurements the optimized rectifier in our prototype outperforms state-of-the-art commercial rectifier chips within desired input power range.	48
3.17 The rectified output voltage as a function of the packet length for different idle times S_{idle} (therefore duty cycles).	49
3.18 The output of Energy harvester (V_{cc} and integrated demodulator (envelope signal). Note that the size of the packet is easily detectable. The WiFi communication rate was fixed to 1 Mbps. harvester's output level is fairly smaller than the peaks of envelope signal. That reason is the long idle times between packet transmissions. The data is captured by a Infinium MSO8104 oscilloscope from Agilent Technologies. The plot is regenerated in MATLAB.	50
4.1 Electromagnetic interactions with biological materials are not yet fully understood.	53
4.2 The components of a simple interface between a cell and a wireless device.	58
5.1 An overview of nanoresonators with electric (right) and magnetic (left) coupling. The viscoelastic properties of the resonators are identical.	70

5.2	Magnetosome arrangement in magnetotactic bacteria. The magnified part shows how elastic protein fibres embed magnetite (Fe_3O_4) crystals in the cytoskeleton. Interaction of the magnetic dipole of the crystal with external fields within its viscoelastic environment can be analyzed by our presented theoretical model as a torsional nanoresonator shown on right hand side. Magnetic torque rotates the MNP around its center of mass. The rotational spring constant is given by $\kappa = kR$, where k is the aggregate rigidity of the connecting protein fibers and R is the radius of the MNP. Since the Reynold number of the MNP is very small, the drag forces are given by Stoke's law. Therefore, the rotational damping coefficient is $C = 6\pi\eta R^3$, where η is viscosity of the surrounding fluid.	75
5.3	(Color online) Quality factor of the resonance for reasonable range of values for the environment viscosity and the rotational spring constant of elastic environment (in terms of $k_B T$). We assume the design includes a magnetite nanoparticle of Radius 100 nm. Note that resonance is possible in the region above $Q = 0.5$ line. It is shown how resonance of a given quality can be achieved in lower frequency by reducing the viscosity experienced by the resonator.	77
5.4	The illustration of the system. (a) an overview of the components of the mechanical nanoresonator at initial (Left) and operating (Right) conditions. Dimensions and angles used in the theoretical analysis are shown. (b) Cross section of the carbon nanotube cantilever.	79
5.5	(Color online) Resonant frequency ω_r (upper graph) and Quality factor (lower graph) for reasonable range of values for MNP radius ($10 \text{ nm} < R < \mu\text{m}$) and CNT length ($5 \text{ nm} < l < \mu\text{m}$). The points located outside the colored region represent overdamped oscillations. Graphs are generated in MATLAB.	83

5.6 (Color online) Optimization look-up graph for a magnetite/(5,2)-CNT resonator operating in water at 60 MHz (blue line) and 300 MHz (purple). Any point on a specific frequency line is a valid configuration for R and l , which results in a resonator with resonant frequency of the line's nominal frequency. Graph is generated in MATLAB.	84
--	----

Chapter 1

Introduction

Communication means imparting or exchanging of information among several parties. One important point, which is often overlooked, is that the parties engaged in any form of communication require a certain amount of energy to send, receive, and process the traveling information. A dead node in a network never receives the message intended for it much like a dead person who will never hear a cry.

Over the last decade, wireless communication networks have achieved major success and emerged as the key technology for enabling the mobile revolution. Providing mobility and accessibility, wireless communication redefines the notion of network and connectivity, and powers a huge range of applications. The speed, capacity and robustness of wireless communication keep improving everyday, but several challenges remain, energy-efficiency being one of the most notable [EHK⁺07, Kir92]. Conserving energy in wireless networks is particularly important, because the wireless nodes are critically dependent on their limited energy resource, that is, their battery. Receiving and decoding a wireless signal normally requires a significant amount of computations. In addition, transmitting wireless messages is one of the most energy consuming tasks in today's computing. Performing such energy-hungry

tasks with low efficiency reduces the lifetime of the nodes and eventually causes node death degrading connectivity and performance of the network. Therefore, several attempts at hardware and software levels have been made to tackle this problem: More efficient batteries with larger capacities have been invented [LOH⁺10]; the power consumption of wireless nodes has been significantly reduced thanks to advances in low-power electronics and new methods of computation such as reversible computing [Ben73]; finally, many energy-aware communication protocols and algorithms that factor in the energy constraints of wireless nodes have emerged [CZB⁺10, SR02, SRS03, RSPS02].

All wireless networks struggle with the energy conservation issue, yet the problem is more evident in certain applications such as Wireless Sensor Networks (WSN). A WSN usually consists of several spatially distributed nodes that monitor or sense a physical or environmental condition, and transmit the collected data via wireless communication. The sensing process generally does not require a lot of energy. In fact, wireless transmission accounts for almost all the node's energy consumption. In most cases, the data collection occurs sporadically or upon an external request. Therefore, continuous operation of a node's radio, which results in fast battery drainage, is not necessary. Current techniques rely on periodically waking the receiver up to synchronize and respond to the requests of a master node [WR08, CK09]. These methods help conserve energy but are far from optimal. Ideally, the radio component of the sensor node should go into a full-sleep (idle) mode that consumes virtually no energy and wakes up only on external requests or events. This can be achieved by integrating a completely passive component that acts as a wake-up circuit and relays the external request to the idle node. The challenge of engineering such a system, which includes software, hardware and communication protocols, is one of the goals of this study.

Having a receiver that consumes *no energy* while being idle is the optimal solution for any of the scenarios mentioned above. Note that this goal can not be achieved by simply reducing the energy consumption of the radio components; rather, the energy consumption should be eliminated when

no communication is taking place. This rules out the use of conventional wireless devices which are basically an ensemble of active electronic boards that consume energy while operating, regardless of how energy-efficient they are. Instead, let us consider the following scenario: Assume that the incoming signal, which carries a certain amount of information, provides the receiver with the energy required to extract the information. On the other end, the receiver simultaneously executes two actions on the signal. First, it converts the energy of the signal into a usable form. Second, it runs the decoding procedure to extract the embedded information. In this case the energy consumption occurs only when there is an incoming signal, and it is fully provided by the transmitter entity. Therefore, the receiver does not rely on any other source of energy.

Another key factor that greatly impacts the energy conservation problem in wireless networks is the physical dimensions (size) of the wireless device. In context of conventional wireless communications, bigger dimensions normally translate to higher battery capacity hence longer lifetime. Also, larger systems can accommodate a larger antenna, which increases the antenna gain and subsequently the quality of both transmission and reception given a fixed energy budget. The problem of energy becomes more severe when the size of the system approaches micro and nano scales. In such extreme scales, devices are inevitably passive because they cannot afford to include a portable source of energy (i.e. battery). Providing a solution for energy problem at these limits is particularly important as it opens up exciting new avenues of possibility for wireless networks. Nanorobotics is one of the areas that could greatly benefit from the solution. Another potential outcome is the possibility to extend the scope of today's wireless communication from electronic devices to include interactions with biological systems. The second part of this research will focus on this aspect of the energy problem.

1.1 Thesis Overview

Combining energy and information transfer is a promising approach that leads to engineering *passive* wireless receivers. There are many communication schemes that provide vast range of throughput, complexity and energy-efficiency. Also, a few mechanisms such as RF energy harvesting have been proposed to transfer energy wirelessly [VRT08, LMF08]. However, combining these schemes presents several challenges. The range and capacity of today's energy transfer methods are very limited, which makes pairing them with normal communication methods difficult and often impossible. In order to have a functional system, we need to carefully optimize, modify or completely revamp the energy and information transfer mechanisms. This includes building more efficient systems using specialized hardware, and devising better algorithms software solutions that exhaust the physical limits of the hardware.

In the case of extremely small systems, the problem shows a radically different face. In such a small scale, there is no room for sophisticated electronic components. Furthermore, especially for biological systems, almost all the information is being exchanged by means of mechanical and biochemical signals, which are of an entirely different nature from electromagnetic signals. An efficient transduction mechanism is necessary to connect these two seemingly different worlds.

In this thesis, we aim to explore several techniques to transfer energy alongside information via a wireless link. We classify our research into the two following studies:

- First, we look into techniques to consolidate the energy and information transfer in wireless networks. We review and compare the energy transfer technologies, provide design considerations and sketch guidelines to implement such functionality. At the end, we present a communication system that allows two-way communication between a commodity smartphone and a passive receiver. The system features a combination

of ultralow-power electronics and RF energy harvesting. We introduce several techniques to increase the efficiency of the information and energy channels, propose novel communication paradigms and protocols optimized for our setup, build prototypes and finally evaluate the system performance experimentally.

- The second part of this work focuses on transferring energy and information to a tiny biological organism through a synthetic interface. We study the enabling technologies that allow us to build such an interface, challenges ahead and the fundamental limits for energy and information transfer. We propose two different approaches to transduce electromagnetic signals to biochemical signals. We provide theoretical results supported by simulation validations.

1.2 Dissertation Organization

The rest of this dissertation is structured as follows:

In chapter 2, we define a model for consolidated energy and information channels in wireless sensor network. We describe the framework for our model and review the building blocks of such model along with its design requirements. This chapter serves as the basis for chapter 3 in which we present iPoint.

Chapter 3 includes a comprehensive design, optimization, prototype and performance evaluation of iPoint, a novel communication system that features a consolidated energy and information channel. This includes the design and characterization of hardware, software and communication paradigms. Several optimization techniques including theoretical analyses and experimental validations are detailed. The results presented in this chapter have been published in [JN10].

In chapter 4, we turn to the problem of energy transfer at nanoscale. First, we present the motivation behind the study and introduce the concept of Bio-enabled Wireless Networks (BWN). We review the fundamentals of

information and energy transfer in biological systems, and the enabling technologies that serve as the building blocks of future BWNs.

Chapter 5 presents a theoretical study that investigates the wireless energy transfer to a nano-scale electromagnetically-coupled resonator. We develop a theoretical model to study such resonators and perform a quantitative assessment of the energy transfer. The results presented in this chapter have been published in [JBN12, JBN11a, JBN11b, JBN11c].

Chapter 6 reviews the related literature. We discuss previous studies in the field, present the state of the art for relevant technologies and identify the similarities and distinctions of our work. Chapter 7 concludes the document and presents the direction for future work.

Chapter 2

Consolidated Energy and Information Channels (CEICh) in Wireless Sensor Networks

In the previous chapter, we argued that combining energy and information transfer may provide an optimal solution to energy conservation in wireless sensor networks. In this chapter, we overview techniques to combine energy and information transfer channels in wireless sensor networks.

2.1 Overview of CEICh

First, we define the framework (model) in which CEICh is being implemented as follows:

- We consider a wireless sensor network whose nodes (devices) perform computations electronically and communicate using Radio-Frequency (RF) signals.
- The network includes two types of nodes: passively-powered receivers, and the energy-provider master node, which we call the source.

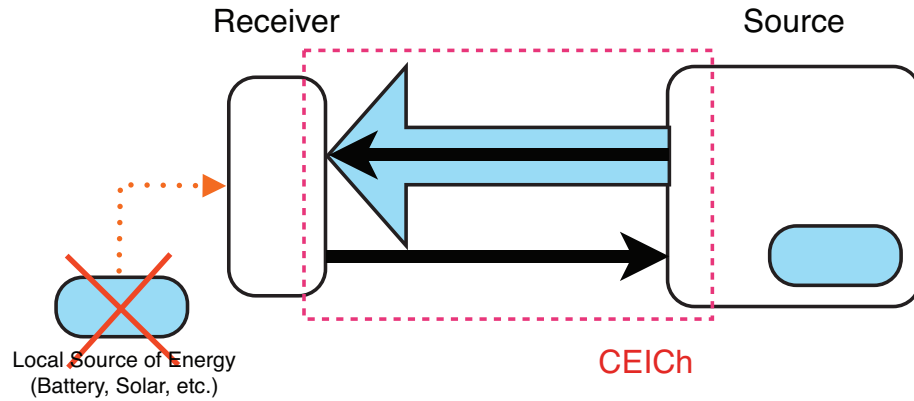


Figure 2.1: The general schematic of CEICh.

- The communication only occurs between a source and a receiver at the time. We do not consider the communication among receiver nodes.
- In order to eliminate the energy conservation problem, the receiver may not rely on a battery or other unpredictable source of energy, such as solar energy or mechanical vibrations.
- In one communication cycle, the source sends the request to the receiver; the receiver receives the request, processes it, computes the reply and sends it back to the source.
- The signal from source to receiver contains both energy and information. The receiver obtains the energy required to receive and decode the transmitted signal from the signal itself. Signals transmitted by receiver are not required to contain energy.

Figure 2.1 illustrates a general schematic of a CEICh.

2.2 Design of CEICh

A CEICh-enabled system performs three tasks: energy transfer, communication and computation. In this section, we take a closer look into the important

features and design elements of a CEICh enabled system.

2.2.1 Energy Transfer Mechanisms

Mechanisms to transfer energy from a power source to a wireless device fall into two categories:

2.2.1.1 Electrodynamic Induction

Methods based on electrodynamic induction use inductive coupling between the source and the receiver, and provide high-efficiency energy transfer over very short distances. In such systems, the efficient energy transfer occurs in the near field region of the source's inductive antenna. The near-field region boundaries are determined by the size of the antenna and the wavelength of the transmission. For smaller antennas, the distances less than a wavelength, $R < \lambda$, from the source are considered near-field region, while the transition to far-field occurs in $\lambda < R < 2\lambda$. For larger antennas, the near-field region boundary is expressed by Fraunhofer distance

$$R < \frac{2D^2}{\lambda}, \quad (2.1)$$

where D is the largest dimension of the antenna. The relationship between transmit power and the distance in the near field can be expressed as follows.

$$P_T \propto \begin{cases} R^{-1} & \text{for } R \leq 0.1\lambda \\ R^{-3} & \text{for } R > 0.1\lambda \end{cases} \quad (2.2)$$

The efficiency declines significantly over greater distances, which makes such methods ineffective when the signal is high-frequency and long-range, a typical case in communications. Recently developed methods apply resonant inductive coupling to achieve much higher efficiency over longer ranges.

2.2.1.2 Electromagnetic Radiation

Methods based on electromagnetic radiation, also called RF energy harvesting, include receivers equipped with *rectenna*, a specialized component made of

an antenna connected to a voltage rectifier that converts the electromagnetic energy of the received signal to a usable DC voltage. These methods operate in far-field region of the corresponding antennas hence attain longer ranges. However, they exhibit a number of limitations. At the antenna level, a system using omnidirectional antennas shows a quadratic drop in efficiency with respect to the distance. Moreover, the losses due to imperfect rectification and antenna matching reduce the efficiency of the system. Matching and rectification losses can be minimized in a well-designed rectenna. Also, the antenna efficiency improves by using directional antennas and applying beam forming techniques.

2.2.2 Energy Transfer Efficiency

The most important property of any energy transfer mechanism is the efficiency, that is what portion of the received energy from the source is converted to usable energy for the receiver side. The factors determining the overall efficiency of an energy transfer system are different depending on the method of transfer.

In case of electrodynamic induction, the overall efficiency is chiefly determined by mutual inductance between the interacting coils, which in general is given by the Neumann formula:

$$M_{ij} = \frac{\mu_0}{4\pi} \oint_{C_j} \oint_{C_i} \frac{ds_i \cdot ds_j}{|R_{ij}|} \quad (2.3)$$

where M_{ij} is the mutual inductance between coil i and coil j , μ_0 is the vacuum permeability, C_i and C_j denote the curve of the coils and R_{ij} is the distance between two points. The final value of the mutual inductance depends on the size of the resonators, their relative orientation and the distance between them. The coupling coefficient between inductive resonators is defined as

$$k = \frac{M_{ij}}{\sqrt{L_i L_j}}, \quad (2.4)$$

where L_i and L_j are self-inductance of the resonators. In many common inductive coupling systems $0 < k < 1$ and the system is called weakly-coupled.

Using recent methods such as *Resonant Inductive Coupling*, one can achieve higher coupling factors ($k > 1$) and build strongly-coupled inductive resonators. Other contributing factors in overall efficiency include ohmic and core losses in the coils, and appropriate impedance matching at either side.

In energy harvesting systems, the overall energy transfer efficiency can be estimated by aggregating the effect of signal's transmission losses, impedance mismatch, and rectifier's energy efficiency. Signal transmission losses are given by Friis equation, which gives P_R , the power received at receiver's antenna:

$$P_R = P_T G_t G_r L_p \left(\frac{\lambda}{4\pi R} \right)^2, \quad (2.5)$$

where P_T is transmit power; G_t and G_r are antenna gains at transmitter and receiver side, respectively; L_p is the polarization loss; λ is the wavelength, and R is the distance between the antennas. Adding the effect of impedance mismatch, we can calculate the power that enters the rectifier circuit, P_{rec} as

$$P_{rec} = (1 - |\Gamma_r|^2) P_R, \quad (2.6)$$

where Γ_r is the reflection coefficient of the receiving antenna. Finally, the input power to the receiver is given by

$$P_{in} = \eta_{rec} \times P_{rec}, \quad (2.7)$$

where η_{rec} is the efficiency of the rectifying circuit. The value of η_{rec} depends on the design of the rectifier (e.g. half-wave or full-wave) as well as the electrical characteristics of its components such as forward and break voltages of the diodes, and leakage voltage of the charging capacitors. In practice, the efficiency of the rectifier is measured experimentally since the exact calculation proves impractical due to complexity and non-linearity of the circuit. In summary, the overall efficiency can be expressed as the following:

$$\eta = \frac{P_{in}}{P_T} = \eta_{rec} G_t G_r L_p \left(\frac{\lambda}{4\pi R} \right)^2 (1 - |\Gamma_r|^2). \quad (2.8)$$

Each of the contributing elements mentioned in (2.8) may be optimized to achieve higher energy transfer efficiency in the design of a CEICh. It is worth

mentioning that (2.8) holds true assuming the perfect channel conditions. In practice, the efficiency is further affected by fading (F^{-1}), shadowing (B^{-1}), and on-object antenna gain penalties (Θ^{-1}), each of which can be either modeled or measured.

2.2.3 Signal Amplification

Another important factor in the design of a CEICh is the minimum voltage required to power-up the receiver, V_{\min} . If the output voltage of the energy transfer unit is not sufficient, a voltage multiplier circuit may be used to elevate the voltage beyond V_{\min} . Because of the limited energy budget, the voltage multiplication is done using a passive circuit. In energy harvesting mechanisms, signal rectification and amplification is done using voltage multipliers.

2.2.4 Voltage Rectification

A voltage rectifier, which is typically a network of diodes and capacitors, rectifies an input AC signal to output DC voltage. The simplest rectifying circuit is the envelope detector circuit shown in Figure 2.2a. Using a diode with forward voltage of V_D , the DC voltage of $V_{\text{out}} = |V_{\text{in}}| - V_D$ can be obtained in no-load conditions. The circuit experiences voltage ripples if connected to a load. This circuit is also called half-wave rectifier because only the positive half of the AC waveform is rectified.

A clamp circuit shown in Figure 2.2b may be used to achieve higher DC voltage levels. The negative half of the waveform is clamped to zero, and the output voltage of $V_{\text{out}} = 2|V_{\text{in}}| - V_D$ is obtained. The circuit, however, shows a very drastic ripple of size $2V_{\text{in}}$ when connected to a load.

By placing a clamp circuit in series with an envelope detector, one can achieve higher DC voltage levels and significantly improve the ripple characteristics of the circuit. This circuit, shown in Figure 2.3, is called voltage doubler and was first invented by Heinrich Greinacher in 1913 and later used to power the particle accelerators [CW32]. Let us look at the steady-state

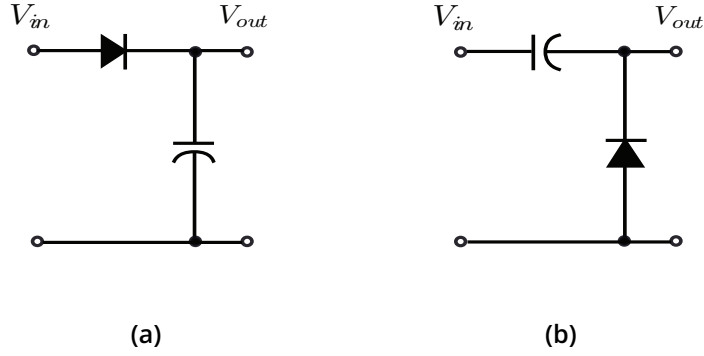


Figure 2.2: The schematics of envelope detector circuit (a) and the clamp circuit (b).

analysis of the voltage doubler circuit. On the negative half of the input AC waveform, the capacitor C_1 is charged until $V_{C1} = |V_{in}| - V_D$. Similarly, over the positive half, the capacitor C_2 is charged until we have

$$V_{out} = V_{C2} = |V_{in}| - V_D + V_{C2} \quad (2.9)$$

$$= 2(|V_{in}| - V_D) \quad (2.10)$$

The key feature of the Greinacher circuit is that individual voltage doublers can be cascaded to build a voltage multiplier that generates arbitrarily large output DC voltage. For an N-stage voltage multiplier the output voltage of $V_{out} = 2N(|V_{in}| - V_D)$ may be obtained theoretically. A output voltage can also be doubled by placing the voltage doubler in parallel with a mirrored copy with the same topology but reversed polarity of the diodes. In a careful design, the amount of ripple can be minimized when connecting the multiplier to a load. Note that the analysis above assumes that the diodes and capacitors in the circuit are ideal in no-load conditions. In non-ideal scenario, the parasitic effect of the capacitors in each stage and non linearity of the diodes significantly affects the performance of the voltage multiplier. Also, the behavior of the components will depend on the output current (load). There is no close form for the efficiency of the system in realistic conditions. Therefore,

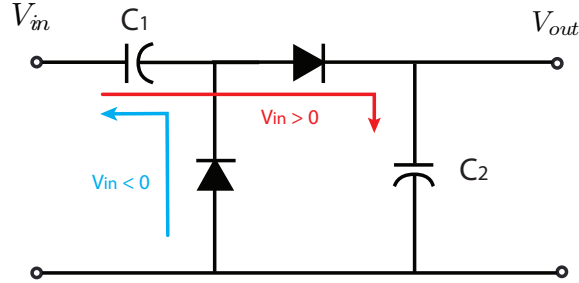


Figure 2.3: Schematic of Greinacher voltage doubler.

the optimization of the overall efficiency of the rectifier should be based on simulation and experimental measurement.

2.2.5 Signal Characteristics

Incorporating energy transfer in communications requires modification in signal characteristics. Unlike conventional communication systems, the receiver does not include an active signal amplifier, therefore the transmitter has to provide a signal with higher level of energy to maintain the receiver in operating zone. In contrast, response signals do not have the aforementioned restriction since the master node does not have any energy constraints and may possess an active radio receiver with signal amplifier to receive and demodulate the response from the receiver.

Signal Preambles, Trailers and Energy Storage

In most cases, the converted power obtained from the signal is not sufficient for continuous operation of the receiver, hence the converted energy should be stored and accumulated over a longer period. In particular, the receiver needs to obtain a minimum amount of energy before it can demodulate the information. Therefore, the signal should include a *preamble* designed to

provide the energy to start-up the receiver. Similarly, having received the signal, the receiver continues to process and respond to the request. The receiver should have already harvested enough energy to complete the tasks, otherwise the signal needs to include a *trailer* that provides the required energy and may contain no actual information. We can define a duty cycle for the system which can be estimated by the following ratio:

$$DC = \frac{P_{ET}}{P_{active}} = \frac{\eta P_T}{P_{active}}, \quad (2.11)$$

where η is the energy transfer efficiency, P_T denotes the power sent by the transmitter, P_{ET} is the converted power from energy transfer unit and P_{active} is the average power that the receiver requires to perform a communication cycle, that is, to start-up, demodulate, process, and reply to the signal. This unavoidable overhead significantly reduces the data rate and throughput of the communications in a CEICh.

2.2.6 Communications Schemes

Because of severe energy constraints, the demodulation process has to as simple as possible, while remaining effective. Sophisticated decoding mechanisms demand a significant amount of computations and energy, hence are not optimal. Due to integration of the energy transfer and communication, the signal from the master node to the receiver carries a considerable amount of energy. Therefore, the signal-to-noise ratio (SNR) is quite high, which allows using simpler modulation and demodulation schemes.

Most of today's communication protocols do not fulfill the requirements mentioned above, thus need to be modified or completely revamped according to the design requirement and constraints. For example, Frequency-Shift-Keying (FSK) and Phase-Shift-Keying (PSK) mechanisms require fairly complex receiver design, hence are not suitable for communication in CEICh. On the other hand, schemes such as Amplitude-Shift-Keying (ASK) or On-Off-Keying (OOK) can be detected by a simpler receiver design (an envelope detector circuit), and consequently can be used in CEICh with minor modi-

fications. Backscattering techniques are used to send information from the receiver to the source. Such techniques based on modulating information in the amplitude of reflected waves adjusting the impedance of the receiver's antenna, allow highly efficient bidirectional communication without using a stand-alone RF transmitter in the receiver. In the following chapter, we present a system that employs a two-way consolidated energy and information channel. The system includes two optimized communication protocols to achieve maximum energy efficiency.

Chapter 3

iPoint

In this section, as an implementation of a CEICh enabled wireless system, we propose a system that provides two-way communication between a receiver with no source of energy and a conventional smartphone. We present a complete design of the system featuring energy harvesting as the energy transfer method. We explore various technologies, introduce new communication paradigms and build a prototype of the passively-powered device that we call *iPoint*.

3.1 Motivation and Possible Applications

Providing information anytime, anywhere, to anybody is a challenging task. Consider an application where we want to deliver information to any person equipped with a standard smartphone in even remote locations where there is no network coverage, and where no source of energy is available. The information should be delivered from a device that can last decades without maintenance. Examples, of applications include information delivery to hikers lost in the woods (e.g., directions, closest points for assistance), caves, and also high-density and interactive information tags (e.g., tourists information, museums).

A smartphone is an ultimate example of a wireless device. It provides a

remarkable combination of data acquisition, computing power and communication interfaces, all in a highly portable package. Our design exploits such capabilities of the smartphone to mitigate energy conservation issues.

3.2 Definition of the System with Respect to CEICh Design

iPoint is a passively-powered device that is capable of communicating with a commodity smartphone while obtaining the required energy for computation and communication from the signal. This completely fits the definition of the receiver in our CEICh model. Here, the master node or the source is a smartphone. In the process of designing the iPoint, in addition to considerations stated in chapter 2, we focused on the following key characteristics:

- *Universality*: any smartphone should be able to serve as the master node without any hardware modifications. Installing a software application should be sufficient to enable all desired functionalities.
- *Interactivity*: the device should be able to accept, process, and reply to specific requests. In other words, the communication between the iPoint and the smartphone is bidirectional.

3.3 Challenges and Approach

The key challenge to implement an efficient CEICh channel is severe power deficiency throughout the system. Smartphones, unlike RFID readers, are not capable of transmitting high power RF signals. In fact, the amount of power transmitted by cell phones is aggressively controlled because of several FCC regulations health issues. Another obstacle that emerges in the course of the design, is lack of specialized wireless interfaces in the smartphone. To maintain the universality of the system, the CEICh design should use one of the standard wireless interfaces of the smartphone (GSM, WiFi, Bluetooth) without any hardware modifications. This eliminates the use of several mechanisms described in chapter 2. For example, inductive coupling energy

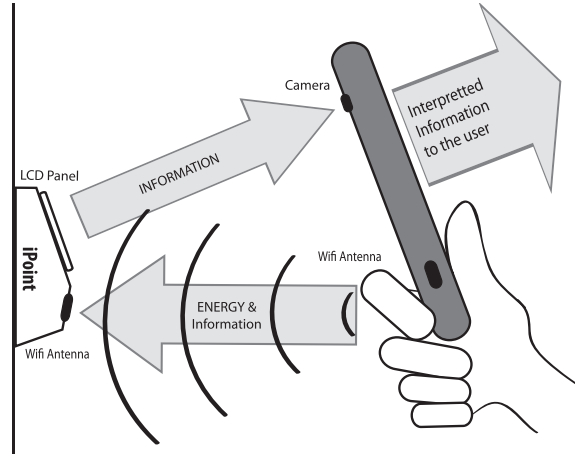


Figure 3.1: Conceptual illustration of how iPoint device performs.

transfer may not be implemented since the majority of smartphones do not include inductive coupling resonator antenna.

3.4 Our Solution

These defining features lead us to a design that introduces innovative communication paradigms and techniques and the integration of a set of fairly unrelated technologies. Among the wireless interfaces present in smartphone, we picked WiFi interface because it provides a greater degree of control by software, works on an unlicensed frequency band (2.4 GHz) and also has the highest transmit power. A backscattering technique cannot be used because of limited power budget and lack of compatible wireless interface to detect the backscattered signal in the smartphone. Instead we design the iPoint to display the result on an LCD panel, exploiting the camera on the smartphone to acquire the data via the captured image of the display and interpret the information. Figure 3.1 shows how this design operates. In the following, we briefly review the system hardware and software architecture, the components, and the communication paradigms and techniques:

- *iPoint components*: the iPoint consists of a rectenna optimized for the

2.4GHz WiFi band, an ultralow-power microcontroller with an LCD-driver and a multi-segment LCD panel.

- *Smartphone*: virtually any smartphone with a WiFi network interface and an integrated camera.
- *Energy-provisioning*: the smartphone delivers the energy to the ipoint via WiFi transmission. The iPoint benefits from a more efficient RF energy harvesting circuit optimized for limited transmission power of smartphones, about two orders of magnitude less than conventional RFID readers.
- *Multimodal communication*: we propose two novel communication mechanisms to circumvent the severe energy asymmetry and constraints.
 - 1) The information from the smartphone to the iPoint is encoded in the WiFi packet width, which results in much simpler and more energy efficient demodulation at the expense of a lower datarate.
 - 2) The information from the iPoint to the smartphone is encoded as a series of patterns shown on the LCD, to be captured by the smartphone's camera.

3.5 Detailed System Architecture

This section outlines the architecture of the proposed system. We describe the system components in detail, discuss the required features, important parameters and trade-offs, and compare design choices. We break down hardware of the iPoint into three components: A rectenna that receives the information and energy, an ultralow-power computing core to process the data, and a display to show the outputs.

3.5.1 Energy Transfer

The energy transfer mechanism in iPhone is based on electromagnetic energy harvesting, therefore consists of a carefully design rectenna. The rectenna serves as the power supply for the device. Its two main components, the

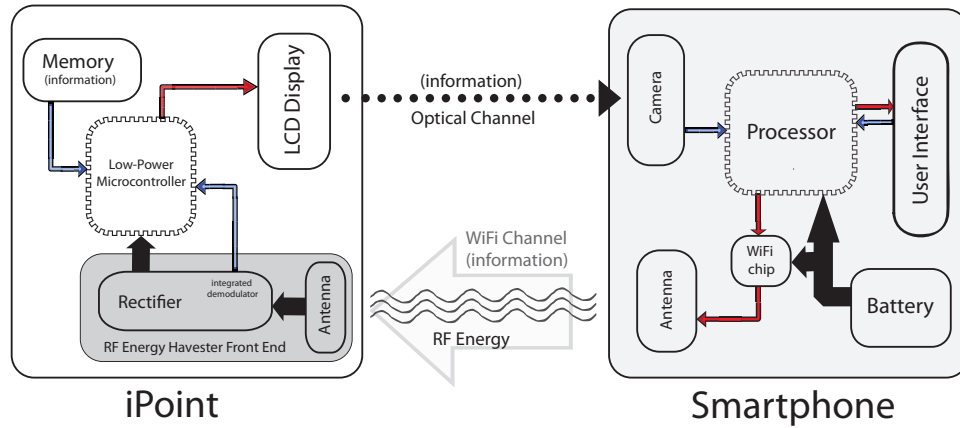


Figure 3.2: Detailed diagram of iPoint.

antenna and the rectifier circuit, in addition to two auxiliary circuits are described below:

- *Antenna:* The antenna is designed for the 2.4 GHz band. External whip antennas provide larger gain and better performance, whereas the integrated printed antenna make more compact design possible. The directionality of the antenna may be adjusted to achieve larger gain given spatial coordinates of the antenna with respect to the smartphone.
- *Rectifier circuit:* It converts the RF energy of the arrived WiFi signals to DC voltage by passing them through a cascade of voltage multiplier circuits. Input power of the rectifier is often extremely small, therefore a multi-stage rectifier is used to build up sufficient output DC voltage, normally 1~5 V, to power the computing unit. The efficiency of the rectifier depends on the overall design of the circuit as well as electrical characteristics of its components, notably forward voltage of the diodes and leakage of the capacitors. A full-wave rectifier shows better converting efficiency and produces more stable DC output compared to a half-wave rectifier, but requires a differential output design. Designs using Schottky diodes, which have smaller forward voltage, and RF optimized capacitors show significantly better performance.

- *Matching circuit:* The antenna and the rectifier should be carefully matched over the WiFi frequency band. Matching is typically done by experiment. The trade-off between a good match and bandwidth of the rectenna should be considered in the design. The ideal bandwidth of the system is roughly 20 MHz, equal to width of the WiFi channel.
- *Regulatory Circuit:* A shunt voltage regulator is placed after the rectifier to maintain the output DC voltage level within the safe range of operation for the computing unit.

Additionally, the rectenna constructs the envelope waveform of the arriving WiFi transmission and passes it, as partially demodulated data, to the computing unit for further processing. We will discuss this in greater detail in section 3.6.

3.5.2 Computation

The computing unit of the iPoint should provide extremely low power consumption along with moderate computing capacity in a simple hardware design. Therefore, ultralow-power Micro-Controllers (MCU), such as TI MSP430 family, are favorable design choices. The MCU should provide an adequate I/O interface and preferably include integrated drivers for external displays. Considering the energy constraints, the MCU may be underclocked to further reduce the power consumption.

3.5.3 Display

The iPoint displays the information with sufficient contrast and clarity to guarantee error-free pattern recognition by the smartphone, and minimize the energy consumption of the process. Passive-matrix Liquid Crystal Displays (LCD) [TKM72] require a very small amount of energy to reach desirable contrasts without the need for a light source on the device, therefore are a better choice compare to LEDs. Given the same input voltage and distance

from the camera, larger panels produce more pixels but less contrast compared to smaller panels.

3.6 Multimodal Communications

Because of the very low-power transmission of smartphones, the energy harvested by the rectenna is not sufficient to power a wireless transceiver and use conventional communication schemes. In this section, we describe two novel schemes that allow two-way communications between the iPoint and the smartphone within such limited energy levels. These schemes leverage smartphone's capabilities to reduce the energy budget of the communications. We break down the communications into two separate channels: smartphone-to-iPoint (S2I), and iPoint-to-smartphone (I2S). We propose a different communication scheme for each channel.

3.6.1 Packet Length Modulation (PLM)

To provide energy for the iPoint device, the smartphone transmits WiFi signals. However, demodulating WiFi packets needs an active demodulator requiring energy beyond what iPoint harvester can obtain from the signals. We propose Packet Length Modulation (PLM), a scheme in which the information is embedded in the length of the WiFi packets.

3.6.1.1 Encoding

In PLM, each packet length represents a symbol in the code. A message is defined as a sequence of WiFi packets each representing its corresponding symbol. Note that the smartphone sends the packets via its WiFi interface, which uses the WiFi protocol and does not know about the PLM. The following modifications to existing WiFi protocol are necessary to implement PLM encoding functionality:

- Since a WiFi access point may not be available, the smartphone creates an ad hoc WiFi network.

- The iPoint lacks any WiFi tranceiver, hence no acknowledgment packet is sent back to the smartphone. Therefore, PLM uses broadcast packets to prevent unnecessary packet retransmission.
- The WiFi packet length depends on the size of the packet, rate of the communication, and fragmentation. To have a robust encoding, the WiFi interface should transmit at a fixed rate without using any rate-adaptation algorithm. This can be achieved by a UDP broadcast transmission.
- Assuming the PLM mechanism uses M different packet lengths, each packet encodes $\log_2 M$ bits of information. The fragmentation threshold determines the maximum packet length, hence the number of the symbols, and should be set to the maximum.

All modifications above are made in the software; no hardware modification is necessary.

3.6.1.2 Decoding

To decode the PLM signal, the iPoint retrieves the length of the received WiFi packets. First, the rectenna generates the envelope signal of the received WiFi packet, and sends it to the computing unit. The computing unit samples the signal, determines its length, and maps it to its corresponding symbol. Predefined start and stop flags can be used to distinguish the beginning and the end of a message. Figure 3.3 illustrates the steps of PLM decoding.

3.6.1.3 Data Rate Analysis

Let M denote the number of the packet lengths in the PLM. Assume the transmitter sends the packets at rate, R . Let S_{\min} be the smallest packet size. S_{\min} is determined by the MCU clock to guarantee packet detection and length estimation, and by the energy harvester efficiency and MCU energy requirements. We consider packets of size multiples of S_{\min} , $S_i = i \times S_{\min}$.

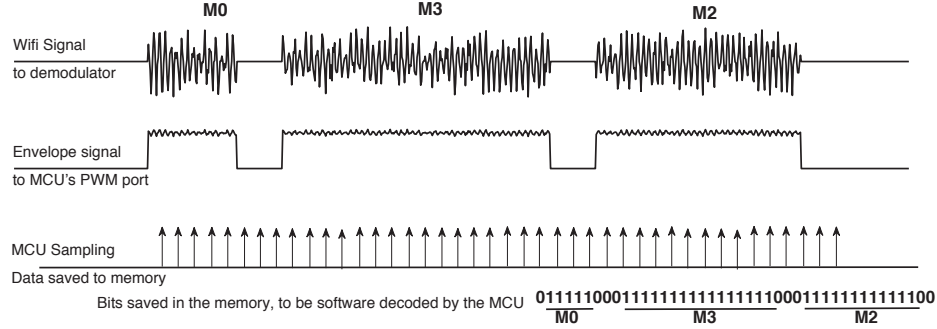


Figure 3.3: PLM decoding.

Hence, the average size of the packet would be

$$S_{\text{avg}} = \frac{S_{\text{min}} + S_{\text{max}}}{2} = \frac{(M + 1)}{2} S_{\text{min}} \quad (3.1)$$

Further assume a message is a sequence of packets separated by *idle* periods of the length S_{idle} . We can calculate the time needed to send a packet, T_p as following:

$$\begin{aligned} T_p &= \frac{S_{\text{avg}} + S_{\text{idle}}}{R} \\ &= \frac{(M + 1)S_{\text{min}} + 2S_{\text{idle}}}{2R} \end{aligned} \quad (3.2)$$

Where R is the data rate of the WiFi transmission in bps. Each packet encodes $\log_2 M$ bits of information. Therefore,

$$R_{\text{PLM}} = \frac{\log_2 M}{T_p} = \frac{2 \log_2 M \times R}{(M + 1)S_{\text{min}} + 2S_{\text{idle}}} \quad (3.3)$$

The values of S_{min} and S_{idle} are determined by the maximum sampling rate of the MCU at iPoint side. Assuming f_{MCU} is the sampling frequency of the MCU, we have,

$$S_{\text{min}}, S_{\text{idle}} > \frac{2R}{f_{\text{MCU}}} \quad (\text{Nyquist theorem}). \quad (3.4)$$

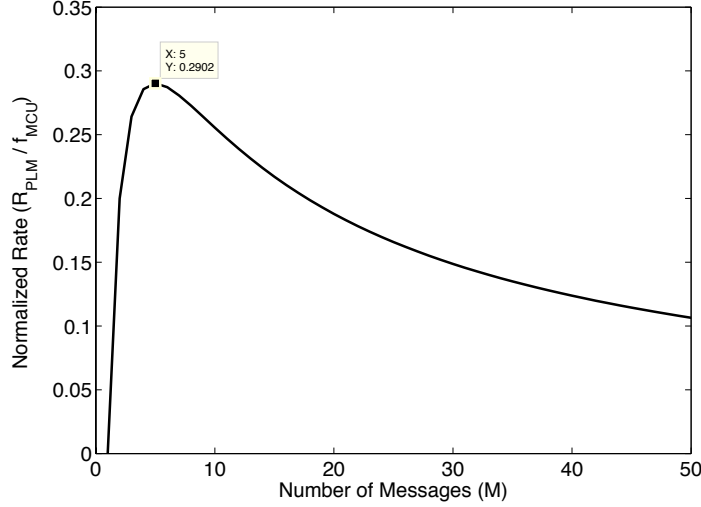


Figure 3.4: Normalized Rate of PLM for different number of messages. It is shown that the best performance is achieved when $M = 5$

Hence,

$$\begin{aligned}
 R_{\text{PLM}} &< \frac{2R \log_2 M}{(M+1)\left(\frac{2R}{f_{\text{MCU}}}\right) + 2\left(\frac{2R}{f_{\text{MCU}}}\right)} \\
 R_{\text{PLM}} &< \frac{\log_2 M \times f_{\text{MCU}}}{M+3}.
 \end{aligned} \tag{3.5}$$

Figure 3.4 illustrates the performance of the PLM for different values of M , showing the best performance is achieved using five different packet lengths. Note that during idle periods, iPoint does not receive energy from the smartphone. This lowers the output voltage of the rectifier which may result in unwanted shut-down of the system. To maintain the harvested voltage level above the desired threshold, S_{\min} needs to be larger than S_{idle} . We define the duty cycle of the PLM as the S_{\min}/S_{idle} ratio. The minimum duty cycle that allows the system to operate continuously depends on the implementation and may be evaluated experimentally. Moreover, $S_{\max} = M \times S_{\min}$ should be smaller than the fragmentation threshold in the smartphone's WiFi interface.

Finally, the smartphone needs to send preamble and trail WiFi packets to

provide the energy required for the iPoint to startup, process the information and send the reply message back through I2S channel.

3.6.1.4 Bit Error Rate of PLM

Before we start to estimate the Bit Error Rate (BER) of the PLM, let us take a closer look at the decoding mechanism. As previously explained, messages are separated with an idle period of length $S_{\text{idle}} = S_{\text{min}}$. Let us assume that MCU records N samples during that period. The sample is considered low (OFF) if the recorded voltage is below a threshold (V_{th}), otherwise is recorded as high (ON). PLM decoder uses a sliding window to detect the S_{idle} while counting the recorded samples. The decoder detects S_{idle} when more than $\lfloor N/2 + 1 \rfloor$ samples in the window are recorded as OFF. Once S_{idle} is detected, the number of the samples up to that point determines the preceding message. Given this decision mechanism, there are two possible scenarios that the decoder receives an incorrect message:

CASE I: If the decoder fails to detect an idle period. In this case, two messages around the undetected idle period are both lost.

CASE II: If the decoder mistakenly detects an idle period in the middle of a message. In this case, the incoming message is lost.

First, we estimate the probabilities of sample error. Because of the close proximity of the communication entities and presence of line of sight, we model the channel between source and the receiver as Additive White Gaussian Noise (AWGN) channel with good approximation. Therefore, the received sample, y can be expressed as $y = s + n$, where n is the noise estimated by a zero-mean normal distribution with variance of N_0 . During the idle period, the input of the envelope detector is the white noise, n . If Gaussian noise is passed through an envelope detector, the probability density function (PDF) of the envelope of the noise at the output of the detector can be estimated

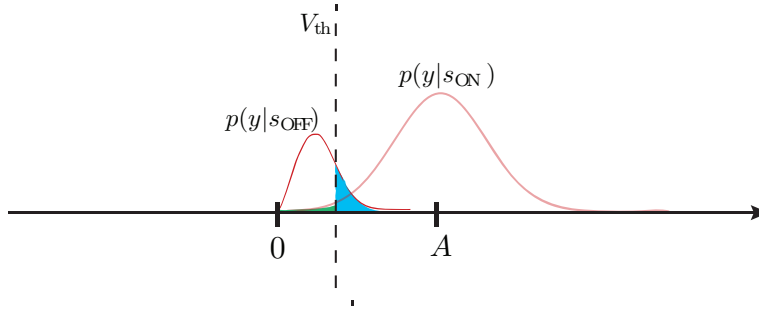


Figure 3.5: Probability density function of the received sample with PLM modulation

with following Rayleigh density function [PS08]:

$$P(x) = \frac{x}{N_0} e^{-x^2/2N_0} \quad (3.6)$$

Therefore, the probability of the error (Blue area shown in Figure 3.5) is given by

$$P(e|s_{\text{off}}) = P(x > V_{\text{th}}) = \int_{V_{\text{th}}}^{\infty} \frac{x}{N_0} e^{-x^2/2N_0} dx. \quad (3.7)$$

When the signal is present, the PDF of the output of envelope detector can be estimated by Rician distribution [Ric]. Assuming that the amplitude of the signal is A , we have

$$P(x|A) = \frac{x}{N_0} e^{-(x^2+A^2)/2N_0} I_0\left(\frac{xA}{N_0}\right), \quad (3.8)$$

where I_0 is modified Bessel function of order zero. The sample error occurs when detected envelope falls below voltage threshold and has the following probability (Green area shown in Figure 3.5):

$$P(e|s_{\text{on}}) = P(x < V_{\text{th}}) = \int_0^{V_{\text{th}}} \frac{x}{N_0} e^{-(x^2+A^2)/2N_0} I_0\left(\frac{xA}{N_0}\right) dx \quad (3.9)$$

Also, samples are independent and identically distributed (i.i.d.). Consequently, the probability of *CASE I*, that is when more than $\lfloor N/2 + 1 \rfloor$ samples that were sent as s_{off} are detected as s_{on} , can be calculated as following.

$$p_I = \sum_{i=\lfloor N/2+1 \rfloor}^N p(e|s_{\text{off}})^i (1 - p(e|s_{\text{off}}))^{N-i}, \quad (3.10)$$

where $p(e|s_{\text{off}})$ is the probability of an error given an OFF sample was transmitted. In *CASE II*, the probability of error in a message of length $m \times S_{\text{idle}}$ is

$$p_{\text{II}}^m = (1 + (m - 1)N) \sum_{i=\lfloor N/2+1 \rfloor}^N p(e|s_{\text{on}})^i (1 - p(e|s_{\text{off}}))^{N-i}. \quad (3.11)$$

The total probability of *CASE II* can be calculated by averaging over all the message sizes. For PLM with M different message we have

$$p_{\text{II}} = \left(1 + \frac{(M - 1)N}{2}\right) \sum_{i=\lfloor N/2+1 \rfloor}^N p(e|s_{\text{on}})^i (1 - p(e|s_{\text{off}}))^{N-i}. \quad (3.12)$$

We assume that the probability of sending ON and OFF messages are equal $p(\text{ON}) = p(\text{OFF}) = 0.5$. Each message codes $\log_2 M$. Therefore, the total BER can be written as

$$\text{BER} = \frac{1}{2} \log_2 M (2p_{\text{I}} + p_{\text{II}}) \quad (3.13)$$

3.6.2 LCD Pattern Coding (LPC)

The smartphone's transmitting power is much lower than a conventional RFID reader (few milliwatts for the smartphone versus few watts for the RFID reader). Therefore, using a similar scheme as passive RFID tags (i.e. back scattering) is not practical. Instead, we introduce LPC, a low cost way of sending information to the smartphone taking advantage of the imaging and computing capability of the phone.

3.6.2.1 Encoding

Having processed the request sent from the user, iPoint encodes the information in a series of LCD segment patterns and displays them on the panel. The smartphone captures the sequence of the patterns with the camera, recognizes the patterns, interprets the information, and finally sends the interpreted data to the user through its own UI. Because all the expensive operations are done on the smartphone side, the encoder/transmitter complexity of the iPoint may

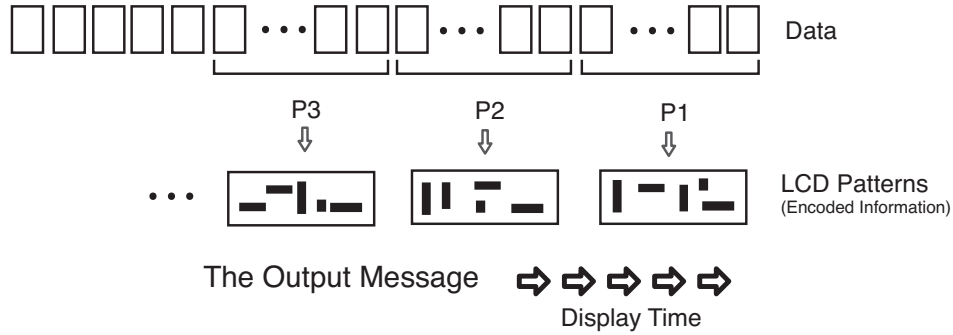


Figure 3.6: LPC Encoding for a M-segment LCD panel.

reduce significantly. This also proves to be a very energy efficient method as displaying information on the LCD panel requires far less energy compared to conventional back scattering scheme used in passive RFID tags. To get an intuition about the energy efficiency of LCD displays, one can think of the lifespan of wrist watches with LCD display; they run for years on a tiny button cell holding a small amount of charge.

An LCD pattern is a combination of the LCD display's segments where a segment can be ON or OFF. Upon receiving a request, the MCU computes the LPC encoded output message, as a sequence of predefined patterns to be shown on the LCD panel. A 2D-barcode encoding such as QR codes may be used to encode the information. An LPC message that consists of n patterns on a M-segment LCD panel, encodes $n \times M$ bits of information.

3.6.2.2 Decoding

At the other end of the channel, the LPC message is captured by the smartphone's camera by either recording a video or taking a series of pictures at a satisfying rate. The smartphone decodes the captured message by running a pattern recognition algorithm on each frame, and sends the interpreted data to the user via UI or uses the data in the next sessions of communication. Several 2D-barcode decoding algorithm and software for smartphones have been published [FK07]. An example of such setting is shown in Figure 3.7.

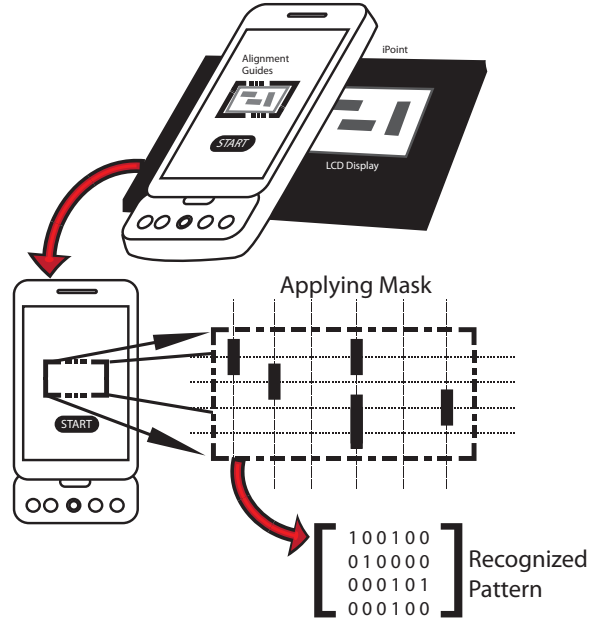


Figure 3.7: LPC decoding. To make decoding faster, the user is asked to align the image of the panel within a virtual box, then the frame is sampled only on the intersections of mask grid-lines (Narrow dashed lines).

3.6.2.3 LPC Rate Analysis:

Using passive-matrix panels, the LCD pattern update rate can go up to 200 Hz. However, our experiments indicate that the deciding factor on an error free decoding is the sampling rate of the camera. Let R_c denote the maximum sampling rate of the smartphone's camera. Applying Nyquist theorem we have, $R_{max} < R_c/2$ fps. Therefore, for a M -segment LCD display, we have the upper bound transmission rate of $R_c M/2$ bps. For most of today's commercial smartphone cameras, $R_c \approx 30$ fps.

3.7 Optimization Techniques

In this section, we take a closer look into the techniques to optimize the performance of the iPoint. We review the design choices for each component

of the system, and present advantages and disadvantages for each design. Also, we study the trade-offs that emerge in the course of the hardware and software design.

3.7.1 Antenna

The antenna is a key component of the iPoint design and its performance has a major impact on the overall efficiency of the system. Note that in any communication system, the design of both receiver and transmitter antenna should be optimized. However, in order to maintain universality in our design, we do not have any control over the transmitting antenna on the smartphone. Therefore, we assume that the smartphone is equipped with an omnidirectional antenna optimized for the WiFi frequency and focus on improving the receiving antenna. In the design of iPoint, we aim to maximize the gain of the antenna as well as its radiation performance over the operating frequency band, which is 2.4 GHz for iPoint. The cost and size of the antenna play an important role in choosing the proper antenna design. There are three main types of antennas that can be used in our design: whip antennas, chip antennas and PCB planar antennas. Whip antennas consist of a single straight piece of conductor, normally in the form of a wire, mounted over the ground plane. These antennas have the simplest design and can achieve high gains (up to ≈ 6 dBi). However, they should extend perpendicular to the ground plane and the board to achieve the best performance hence are not easily fit in compact board designs. Chip antennas are smaller and can be easily mounted on electronic boards, but have a radiation performance ranging from mediocre to poor. PCB antennas provide the most flexibility in terms of antenna geometry. They are planar and have small size in high frequencies therefore can fit in compact designs. The RF performance of the PCB antennas are typically worse than whip antennas, but a good performance can be achieved with a careful design using microwave simulation tools. In the following, we present three PCB antennas that we designed for iPoint. We list the characteristics, advantages, and disadvantages of each design.

3.7. Optimization Techniques

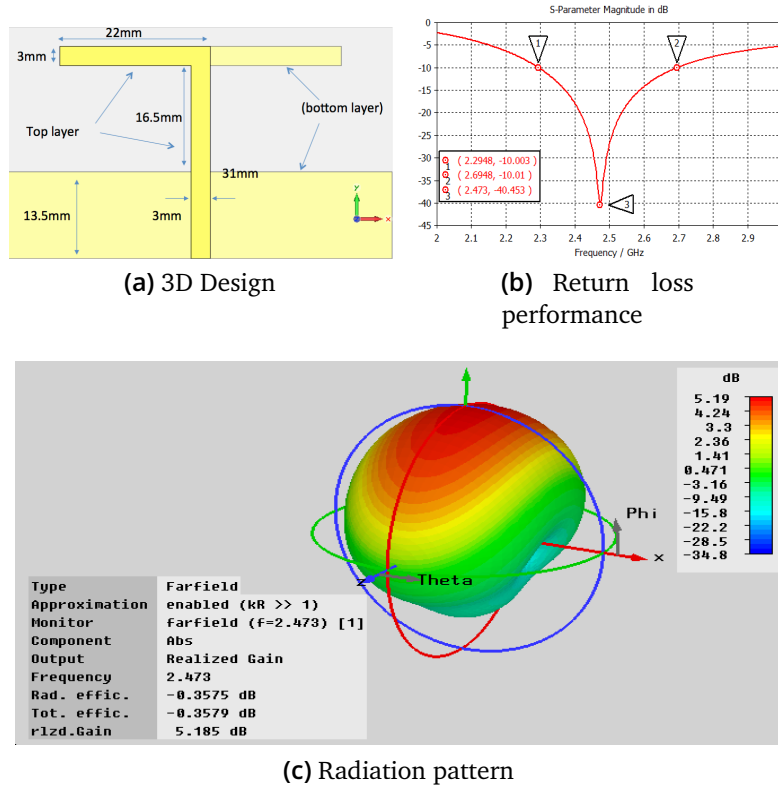


Figure 3.8: The design of the dipole antenna optimized for 2.4 GHz.

3.7.1.1 PCB Dipole Antenna

Dipole antennas have been widely used since the early days of radio. Simplicity and effectiveness for a wide range of communication needs are the reasons for this. A dipole, which it gets its name from its two halves, is a balanced antenna, meaning that the poles are symmetrical: they have equal lengths and are extended in opposite directions from the feed point. To be resonant, a dipole must be electrically a half wavelength long at the operating frequency. Figure 3.8a shows the geometry of our dipole antenna which is designed to operate at 2.4 GHz. The return loss S_{11} of this antenna is presented in Figure 3.8b.

3.7.1.2 Yagi-Uda Antennas

Higher gain antennas are usually obtained by forming arrays of basic antennas. The Yagi-Uda antenna is the most successful general-purpose directional antenna design at frequencies up to 2.5 GHz. It is inexpensive and simple to construct, and will provide gains of up to about 17 dBi. Yagi-Uda antennas can be built to support high input powers, and they are commonly used for directional broadcast transmission. The geometry of the designed Yagi-Uda antenna, which is operating at 2.4 GHz, is shown in Figure 3.9a. The return loss of this antenna is also illustrated in Figure 3.9b. The gain and directionality of Yagi-Uda antennas are particularly desirable. However, their large size in our operating frequency becomes problematic and renders their use impractical.

3.7.1.3 Planar Inverted-F Antenna

The planar inverted-F antennas (PIFA) are commonly used in mobile communication devices due to their small size (quarter-wavelength). These antennas typically consists of a rectangular planar element located above a ground plane, a short circuiting plate, and a feeding mechanism for the planar element. The Inverted-F antenna is a variant of the monopole where the top section has been folded down so as to be parallel with the ground plane. This is done to reduce the height of the antenna, while maintaining a resonant trace length. This parallel section introduces capacitance to the input impedance of the antenna, which is compensated by implementing a short-circuit stub. The stub's end is connected to the ground plane through a via. Figure 3.10a shows the geometry of a PIFA designed to operate at 2.4 GHz. The return loss of this antenna is also shown in Figure 3.10b. PIFA's size makes it a very good choice for compact board design, however its performance is subpar compared to dipole and Yagi-Uda antennas.

3.7. Optimization Techniques

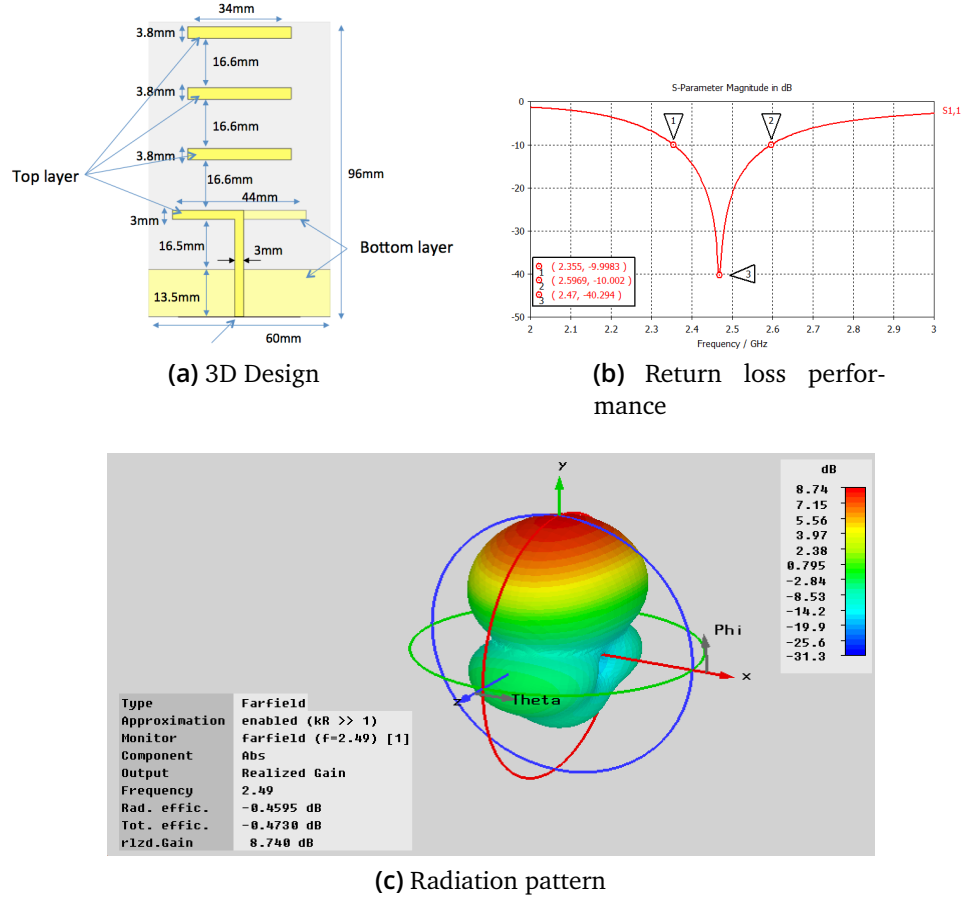


Figure 3.9: The design of the Yagi-Uda antenna array optimized for 2.4 GHz.

3.7.2 Rectifier

The rectifier designed for iPoint is based on multi-stage Greinacher circuit described in section 2.2.4. The overall efficiency of the rectifier is determined by combination of the design of the rectifier and the electrical characteristics of its components. In this section, we review the key elements in designing an optimized rectifier for iPoint.

3.7. Optimization Techniques

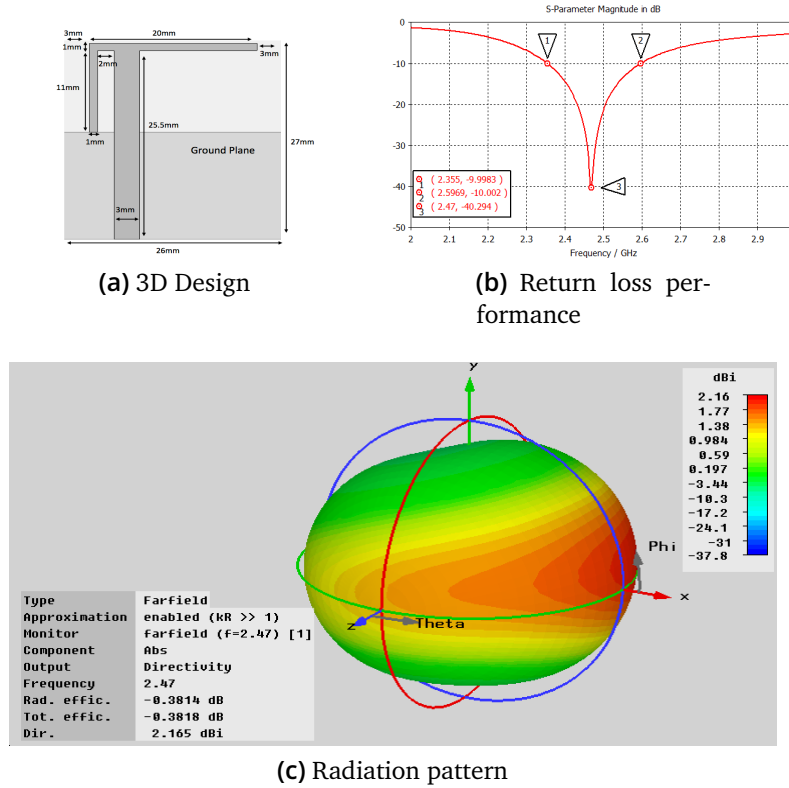


Figure 3.10: The design of the Planar Inverted-F Antenna optimized for 2.4 GHz.

3.7.2.1 Diodes

Since the rectifier is used to convert high-frequency WiFi signals, the diode used in the design should have fast switching times. Among available types of diodes, Schottky diodes provide the fastest switching time, therefore are most suitable for RF energy harvesting. Another benefit of using Schottky diodes is their low forward voltage (150–350 mV), which is considerably lower than normal p-n junction diodes (0.6 V). The lower forward voltage allows a greater portion of the signal to be rectified and directly improves the efficiency of the rectifier. Other important parameters that need to be considered in picking the proper diode for the design are the saturation

current, junction capacitance, and series resistance. In particular, we are looking for the following characteristics:

- High saturation current is required for driving heavier loads.
- Lower junction capacitance leads to lower overall rectifier reactance and reduces the frequency dependence of the rectifier, and consequently eases the impedance matching.
- Lower series resistance is desirable in order to reduce the power loss within the rectifier.

In our prototype, we use HSMS-282x schottky diodes from Avago Technologies since they provide the best combination of the electrical characteristics within the operating frequency and power band.

3.7.2.2 Load Impedance

As described before, the Load impedance greatly affects the performance of the rectifier. The impedance of the MCU computing core of the iPoints varies depending on the state of the computation. The Low power mode (LPM) of the MCU shows the highest impedance, whereas the lowest impedance was measured when MCU was driving the LCD. The highest power consumption coincides with the lowest impedance of the MCU, measured as 140 k Ω ; In order to ensure that the rectifier provides necessary power at all times, we modify the rectifier to have the best efficiency while driving the maximum load.

3.7.2.3 Rectifier Topology

The number of the stages and RF input of the rectifier have significant effect on the output voltage level and efficiency of the rectifier.

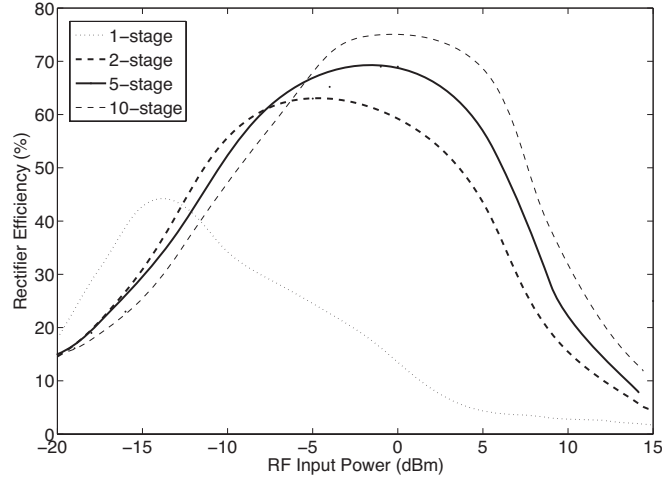


Figure 3.11: Rectifier efficiency versus Input power for different number of the stages.

Number of Stages In an ideal multi-stage rectifier, the output voltage is proportional to number of the stages. Nevertheless, that doesn't hold in practice. The parasitic effects of the intermediate stages plus the power loss due to resistance in each stage limits the practical number of stages. Because of the complexity of the issue, the accurate analytical calculation is not practical, but the optimization can be done using realistic simulation. We used Agilent ADS tool to simulate rectifiers with different number of stages. The components of each circuit are identical and simulated using the vendor-provided parameters. Figure 3.11 shows the efficiency of the rectifiers vs input RF power. It shows that the maximum efficiency of the rectifier improves as number of stages grows. The simulation result also shows that rectifiers with higher number of stages show better efficiency at higher input powers.

3.7.3 Matching Strategy

The goal of the matching network is to adjust the input impedance of the system seen from the antenna-rectifier interface, Z_{in} , in order to have

$$Z_{in} = Z_{ant}^*. \quad (3.14)$$

Here lies a peculiar problem: the diodes are non-linear electrical components, hence the rectifier circuit shows a collective non-linear behavior. This implies that Z_{in} depends on the input power from antenna, P_R . This is not an ideal situation because P_R may vary unpredictably due to numerous dependencies discussed in section 2.2.2. The dynamic input impedance calls for a dynamic and adaptive matching mechanism that cannot be achieved using passive components.

A viable solution to minimize the effect of impedance mismatch is to measure the variation of Z_{in} for a reasonable range of input power and design the matching circuit accordingly. In the case of iPoint, we assume that the smartphone is always transmitting WiFi signals at the maximum power allowed by regulations. Therefore, the optimal matching occurs when the communication occurs in a specific distance, which can be predicted.

The problem of dynamic impedance remains even if the input power is constant. This is because the input impedance of the system is also affected by the current that computing unit draws from the rectenna, i_{out} . For example, the MCU requires significantly higher current in the active mode (i.e. performing computation) compared to standby (i.e. Low-power mode), which results in lower input impedance. If matching is optimized for the standby mode, any increase in i_{out} results in quick drop of output voltage of the rectifier leading to system shutdown. A partial solution is to match the rectenna for a desired input impedance, which in most cases is minimum value of Z_{in} when $i_{out} = max$. Given a fixed input power, when i_{out} falls below maximum value, a power mismatch occurs but in fact the output voltage of the rectifier increases. This prevents the system from shutting down as long as the input power is sufficient.

In our design, matching is done using a LC network plugged between the antenna and the rectifier. The final trade-off in matching is the operating bandwidth of the system. While high-quality sharp matching maximizes the power transfer efficiency, it also makes the system more frequency selective. This might not be ideal where the operating bandwidth of the system is not small. The fundamental limit of impedance matching over a bandwidth can be estimated by Bode-Fano theorem. Let us assume the rectifier circuit can be represented by a parallel RC network. According to Bode and Fano, if a lossless matching network is employed, we have the following limit on the reflection coefficient for different frequencies:

$$\int_0^\infty \ln\left(\frac{1}{|\Gamma|}\right) d\omega \leq \frac{\pi}{RC}. \quad (3.15)$$

A perfect matching over a specific bandwidth $\Delta\omega = \omega_2 - \omega_1$ is theoretically achieved if $\Gamma = 1$ for frequencies outside the bandwidth and $\Gamma = \Gamma_{\min}$ for $\omega_1 < \omega < \omega_2$. Equation (3.15) gives the following lower bound for operating reflection coefficient:

$$\Gamma_{\min} > e^{-\pi/RC\Delta\omega}. \quad (3.16)$$

Dynamic impedance of the system makes the matching mechanism a very complex problem. As previously explained, the efficiency of the rectifier is also dynamic and shares some of the same dependencies. In practice, it is necessary to determine the value of matching components by optimizing the output power of the rectenna, which accounts for both matching and rectifying efficiency. Figure 3.12 shows the performance of the designed matching network for iPoint's rectenna.

3.7.4 Low-power Computation

3.7.4.1 Power-aware Software

The embedded software of the iPoint takes advantage of low-power modes (LPM) provided by MCU to minimize the power consumption. Any MCU

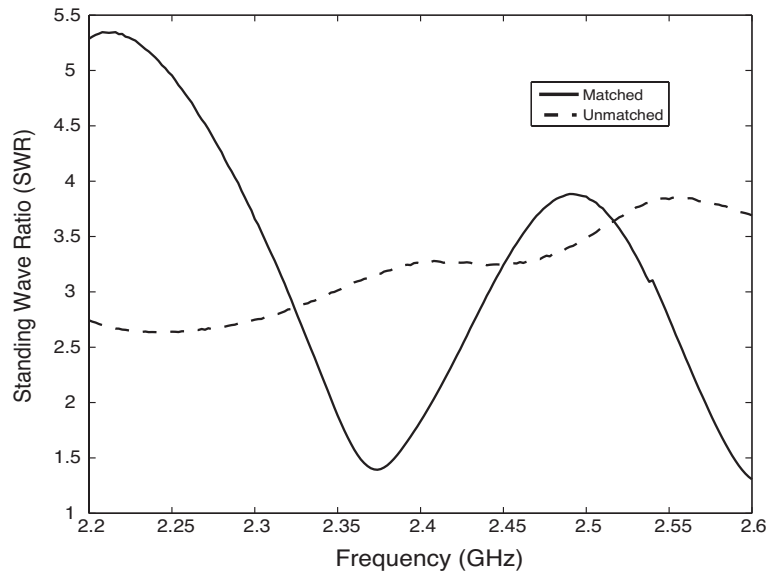


Figure 3.12: The impedance matching in action. The standing wave ratio (SWR) of the rectenna is shown before and after careful matching at active mode load.

components (timer, ADC, etc.) can be turned off, when its functionality is not required.

3.7.4.2 Underclocking

To further reduce the power consumption of the computing core, we aggressively underclock the MCU. The iPoint’s computing core tasks, such as PLM decoding and LPC encoding, do not demand a very fast clock, hence the clock frequency may be reduced to a few kilohertz. Figure 3.13 illustrates the results of our measurements of the MCU’s power consumption running the same instructions at different clock frequencies.

3.8 Prototype

We prototyped different versions of the iPoint based on the design described in Section 3.5. Two versions (Ver. 2.1 and 3.1) are shown in Figure 3.14. In

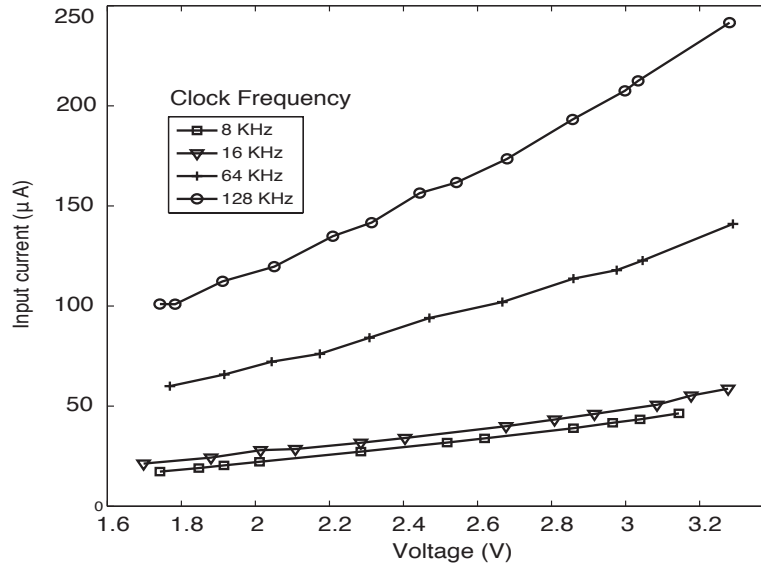
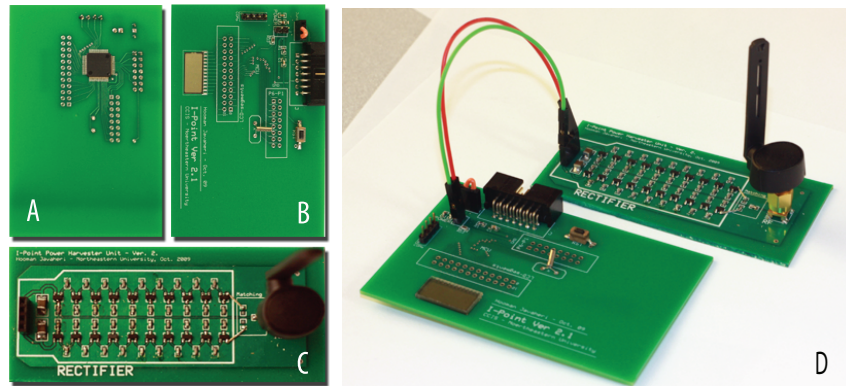


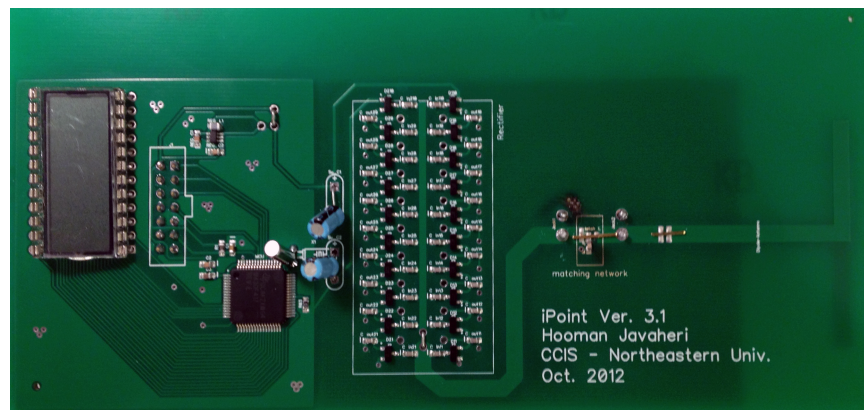
Figure 3.13: Power consumption of MCU for different clock frequencies.

this section, we explain the implementation of the components in detail.

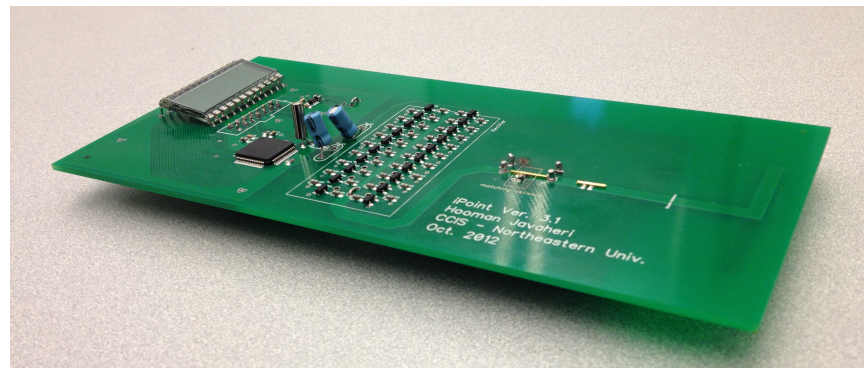
The smartphone used in the experiments is the *HTC Dream* also known as *T-Mobile G1* running Android mobile device platform Ver. 1.6. This 3G phone is equipped with a 528 MHz Qualcomm ARM11 Processor, 192 MB of DDR SDRAM, 320×480 pixel LCD Display with 180 ppi, 3.2 megapixel camera with auto-focus capability, and a WiFi (802.11 b/g) wireless interface [HTC]. We developed a software application in Android platform that sends multiple PLM-modulated requests, and performs the LPC decoding. The WiFi interface was configured to send broadcast packets at a fixed rate of 1 Mbps, the lowest rate supported by WiFi communication. Ideally, the application should create an ad hoc network, but the Android's support for the ad hoc mode is currently limited. As an alternative solution for prototyping, the smartphone connects to an auxiliary WiFi network created by an external access point. We use UDP/IP, as opposed to TCP/IP, to avoid unnecessary retransmissions caused by TCP flow-control mechanism. For the iPoint's rectenna, we implemented a 10-stage modified Greinacher circuit, a full-wave rectifier with parallel RF



(a) The iPoint prototype boards: A) Computing core upper layer (LCD display is shown). B) Computing core lower layer (MSP430 is shown). C) RF energy-harvester front end, 10-stage Greinacher voltage multiplier. D) The realization of iPoint version 2.1.



(b) Prototype Version 3.1 with unified board design and PCB antenna.



(c) Low-profile design of the iPoint Ver. 3.1

Figure 3.14: The Prototype of iPoint.

inputs connected to a 2.4 GHz whip antenna. We used high-performance low-leakage RF capacitors, and schottky diodes (HSMS-282 series from Avago technologies) with forward voltage threshold of 150~200 mV, the lowest available. The value of intermediate capacitors were chosen experimentally to maximize the output DC voltage. The rectenna then was matched on WiFi channel 1 (2.412 GHz) using an LC matching network. The first stage of the rectifier circuit was used as an envelope-detector circuit for PLM decoding. For the communication core, we embed a TI MSP430F417, an ultralow-power microcontroller from Texas Instruments. This 16-bit flash MCU provides desired computing capabilities at low power consumption. It features 32 kB + 256 B of flash memory, 1 kB of RAM, Low supply voltage of 1.8 V, integrated LCD driver for 96 segments, on-chip comparator that can be used for finalizing the PLM signal demodulation, and very low active power consumption of 200 μ A at 1 MHz, which makes it a reasonable choice for the iPoint prototype. The LCD panel selected for this generation of prototyped device was a 26 segment watch LCD display.

3.9 Performance Evaluation

We carried out several experimental measurements in order to accurately characterize the prototyped device and prove the functionality of the design components. This section presents the detailed description of the testbed and experimental results.

3.9.1 Range

Based on our experiment, iPoint requires around -10 dBm of power to operate normally. The transmit power of WiFi interface of smartphones varies from a model to another but can be roughly estimated between 10–20 dBm. If the antennas at both receiver and transmitter side provide gain of $G_T = G_R \approx 3$ dB, and we have polarization mismatch of $L \approx -3$ dB, the link budget analysis gives an operating range up to two times of the signal wavelength, which is

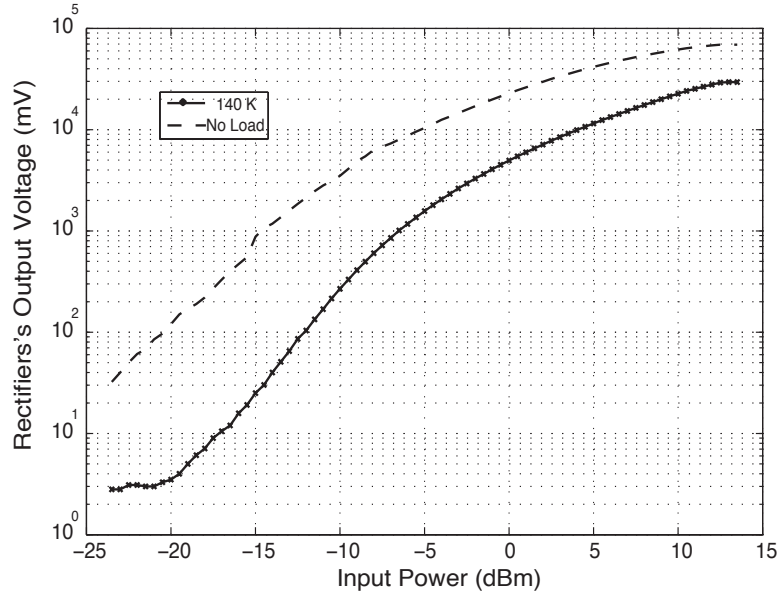


Figure 3.15: Performance of the energy harvester unit.

12.5 cm for WiFi signal. Our experimental evaluation is in agreement with the preceding estimation; our prototype was fully operational in ranges below 25 cm.

3.9.2 Rectifier Efficiency

To characterize the efficiency of the rectifier circuit, a MXG Vector Signal Generator was used to feed the rectifier via a 0.5 feet coaxial cable, and the output voltage level of the rectenna was measured. The rectifier was fed with a WiFi signal in a wide range of input power, from -20 dBm to 15 dBm. The output voltage and efficiency were measured without a load and with a load of 140 k Ω , which is close to the MCU impedance in active mode. Rectifier shows efficiencies up to 72%. The results are shown in Figures 3.15 and 3.16.

3.9.3 Duty Cycle of PLM

Minimum duty cycle as one of the important characteristics of the iPoint system was discussed in section 3.5. We measured the output DC voltage

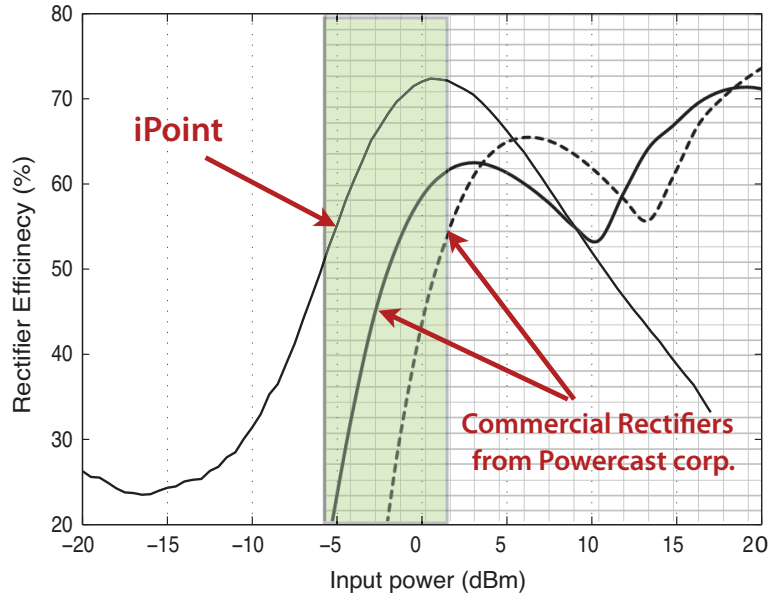


Figure 3.16: Energy-harvester efficiency as a function of input power. The shaded region indicates the operating range of the iPoint. Based on our measurements the optimized rectifier in our prototype outperforms state-of-the-art commercial rectifier chips within desired input power range.

of the rectenna for different duty cycles. The results are summarized in figure 3.17.

3.9.4 LCD Contrast Test

The accuracy of LPC decoding relies on the contrast of the pattern shown on the LCD panel, light conditions and the distance of the camera from the panel. If available on the smartphone, an LED flash may be used to compensate low-light conditions.

The power consumption of two LCD panels with different sizes were measured: Panel 1 (3 cm², 24 segment), and Panel 2 (1.8 cm², 26 Segments). A test image was taken from the LCD panels at the same distance and under the same light environment while the same pattern were displayed on both panels. The contrast of the panels were compared digitally in Adobe Photoshop. To

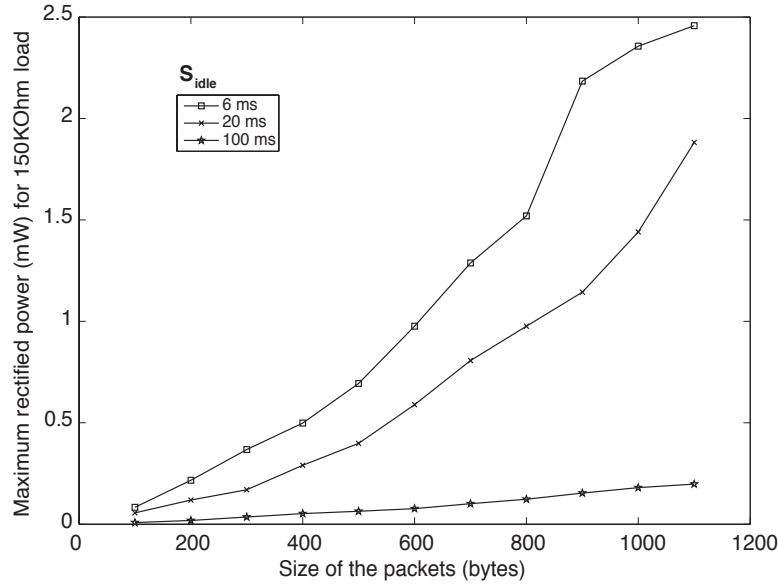


Figure 3.17: The rectified output voltage as a function of the packet length for different idle times S_{idle} (therefore duty cycles).

create a given desired contrast, we measured the required voltage and input current for each panel. The Larger panel, requires 2.9 V drawing 49 μA (142.1 μW), whereas Panel 2 requires 1.9 V drawing 21 μA (39.9 μW).

3.9.5 PLM Decoding Performance

In order to test the functionality of the integrated demodulator of the front end, packets with different sizes were sent over the WiFi channel by the smartphone while the output of the energy harvester and integrated demodulator being measured. The rate of communication was fixed to 1 Mbps. The result is shown in Figure 3.18.

3.10 Conclusive Remarks

In this chapter, we introduced iPoint, a device that can interact with commodity smartphones, equipped with a WiFi network interface and camera, therefore enabling ad hoc and universal communication. The energy and infor-

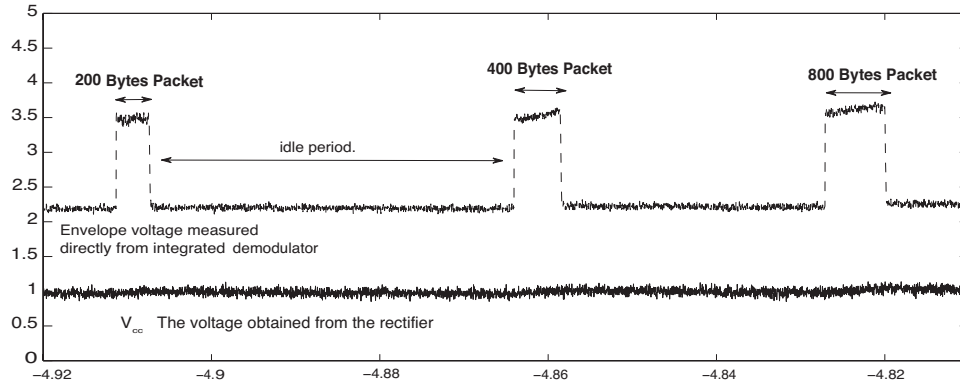


Figure 3.18: The output of Energy harvester (V_{cc} and integrated demodulator (envelope signal)). Note that the size of the packet is easily detectable. The WiFi communication rate was fixed to 1 Mbps. harvester's output level is fairly smaller than the peaks of envelope signal. That reason is the long idle times between packet transmissions. The data is captured by a Infinium MSO8104 oscilloscope from Agilent Technologies. The plot is regenerated in MATLAB.

mation are exchanged in an instance of a previously described CEICh channel. At the core of iPoint lies an ultralow power microcontroller. iPoint draws the integrality of its energy from the smartphone transmissions, through an RF energy-harvester, making the use of batteries unnecessary and guaranteeing its longevity. Two new communication paradigms are introduced:

- Packet Width Modulation allows the smartphone to encode information in the width of the WiFi packet and making demodulation extremely energy efficient
- LCD information encoding and camera decoding.

We discussed several design possibilities and built a prototype of the iPoint. We reported on the performance of our system for various transmission powers, operation frequencies of the microcontroller, packet sizes and duty cycles.

Chapter 4

Energy and Information Transfer in Bio-enabled Wireless Networks

While energy efficiency remains one of the main challenges in wireless networks [EHK⁺07, Kir92], biological systems are well known to be extremely energy efficient. From the brain, which performs outstandingly complex tasks with only a few tens of Watts, to the ear, which can carry out the equivalent of a billion floating-point operations per second, biological systems are many orders of magnitude more efficient than our state of the art wireless systems. Such an efficiency gap can be explained by the fact that today's electronic systems rely on transistors ($\sim 30\text{nm}$) to perform very basic functions, while biological systems rely on nano-level machines (e.g., proteins) to perform specialized and complex functions. A natural, although clearly challenging question is if we can build biologically-enabled wireless networks. Note that the theme of this research is bio-enabled mechanisms which are fundamentally different from bio-inspired techniques in which the functionality of the electronic device is inspired by an existing natural mechanism. This quantum leap in efficiency is analogous to the improvements from Pascal's mechanical calculators to electronic calculators. We argue that recent advances in bio-engineering technology and synthetic-biology will dramatically expand the frontier of wireless communication research.

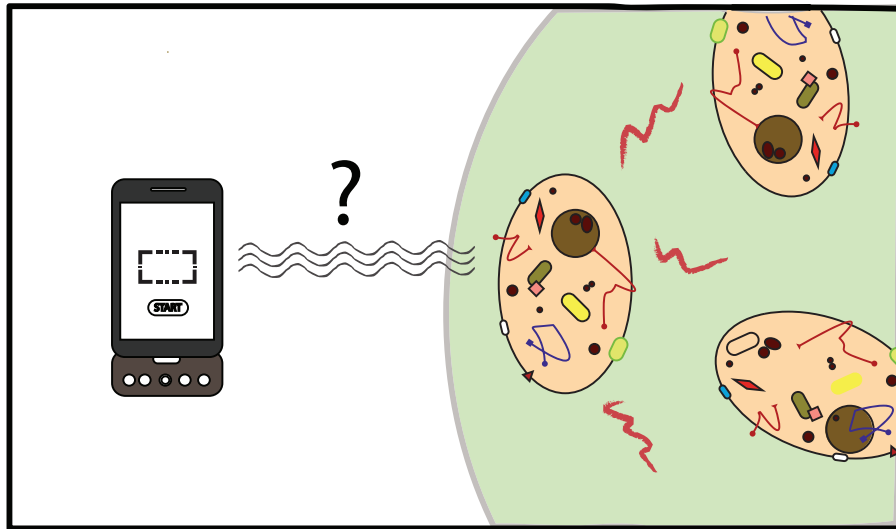


Figure 4.1: Electromagnetic interactions with biological materials are not yet fully understood.

An example of systems that can benefit from such research is a wireless sensor network. Most wireless sensor nodes rely on a periodic wakeup to be paged for requests. This results in significant energy consumption and increased delay. A Bio-enabled Sensor Network (BSN) composed of a nano-power sensing device that can go into a full sleep mode but can still be woken up using a fairly long-range RF signal could solve this problem. The idea is to transduce a weak Electro-Magnetic (EM) signal into biological signals and use a biological device to demodulate the information embedded in the original EM signal [JNN09].

A second application is the engineering of bio-agents that can synthesize and self-assemble a protein/polymer-based radio receiver (such as the recently demonstrated nano-radio [JWGZ07]), that diffuses through the body and targets specific cells such as cancerous cells, liver cells, or even neurons (by generating anti-bodies that binds to targeted membrane proteins [Dob08, Che08]) to allow the remote monitoring, manipulation (e.g., opening/closing ion channels as demonstrated in the remote control of *C. Elegans* worms [HDZ⁺10]), and even destruction (e.g, by triggering apoptosis

processes) of the targeted cells.

An exciting challenge at the frontier of three research communities, namely communication networks, bio-physics, and synthetic biology, is how we can design a wireless communication system that:

- *Interfaces* with bio-organisms for medical applications such as remote control, and monitoring of cells.
- *Leverages* bio-computation and communication for efficiency.

Building bio-enabled wireless communication systems requires overcoming several challenges.

- *Signal propagation*: is challenging because bio-materials severely limit the propagation of wireless signals (e.g., electrical fields are highly attenuated) [POM10].
- *Interfacing*: controlling bio-physical processes is difficult as these processes are still not well understood, and sensing and extracting bio-signals to the external world is not easy using non-invasive self-assembling devices.
- *Size*: devices should be small enough to interface with bio-mechansims at the molecular level.
- *Robustness and stability*: bio-organisms are very sensitive to the environment and need to be engineered for extreme environments[ZSB⁺06].
- *Health*: the proposed technology should be safe to people and the environment.

4.1 Basic Concepts

Connecting two seemingly different worlds requires detailed understanding of their similarities and differences. While biological organisms seem to completely differ from electronic circuits used to built wireless networks, a closer

look at these complex systems reveals a few fundamental similarities. This section presents an overview of the biological world from systems perspective and breaks down some of its important characteristics:

4.1.1 Information Flow and Biological Sensitivity

In systems biology, an organism can be viewed as a complex network of its cells. A cell is a well-defined biological entity able to receive (sense), process, and generate information. In this biological network, information travels using *bio-signals*. Bio-signals exist in the form of mechanical, chemical, or in some cases electrical signals. Examples include pressure, signaling molecules such as hormones, ion concentration change, and electrical pulses produced in neurons. From systems perspective, there are three types of bio-signals.

- *External stimuli*: the information perceived by the cell from the extra-cellular micro-environment. These signals activate a specific receptor (i.e. a protein located on the cell membrane) on the cell and trigger a reaction.
- *Intracellular signals*: intermediate signals produced inside the cell in the process of creating the response. These steps normally include numerous chemical reactions and protein-protein interactions.
- *Cell responses*: the output generated by the cell, which alters the state of the cell or the extracellular environment.

The process by which a cell generates a response to an external stimuli is called *signal transduction*, and the sequence of steps required to complete the process is referred to as *signaling pathway* [NRB08]. The correct execution of the transduction relies on availability of necessary proteins in the cell. Cells produce such proteins using information encoded in their genetic code. The biological behavior of the cell in an environment depends on the variety of its signaling pathways. In multi-cellular organisms, the complex network of signaling pathways coordinates the function of the organism as

a whole. Understanding the information flow in signaling pathways allows the use of a bio-organism as a tool for computation and communication. In addition, advanced *synthetic biology* and *genetic engineering* techniques have made it possible to design and engineer new signaling pathways with enhanced functionality [SEK08]. The sensitivity of a cell to external stimuli is determined by the variety of its receptors, special proteins that normally reside on the cell membrane. Receptors are classified by the stimuli to which they are sensitive, as well as the signaling pathway they trigger. External stimuli include temperature change, mechanical stress and strain, signaling molecules, or a change in electrochemical voltage in the environment.

4.1.2 Speed

Signal transduction execution time depends on the complexity of the pathway and varies for different cell responses. A change in sodium ion concentration in neurons completes in a few milliseconds while a complicated process such as gene expression might take days to finish [NRB08].

4.1.3 Energy

Natural selection has forced bio-organisms to maximize their energy efficiency. Biological organisms show superior energy efficiency compared to today's ultra-low power electronics. As an illustrative example, human brain consumes 20–30 watts of power, less than a third of most advanced CPU designs [Dru00]. Also, ears and eyes outperform the state-of-the-art sensors at the same level of energy consumption.

4.1.4 Complexity

Even in the simplest form (i.e. single-cell), bio-organisms manage to perform a variety of complicated tasks. The ability to produce a vast number of proteins with different functionalities permits bio-organisms to extend the complexity of their actions while preserving their size and efficiency.

4.2 Approach

In a biological system, each cell can be modelled as a Multiple Input Multiple Output (MIMO) device where inputs and outputs denote external stimuli and cell responses, respectively. On the wireless side, a wireless node exchanges the information with its surroundings using high-frequency electromagnetic (EM) signals. Depending on the communication scheme, information is encoded in amplitude (energy level) or the frequency of the signal. An interface should provide an efficient channel to exchange *information* and *energy*. It should not perturb the functionality of either side, which is particularly important for the biological entities because of their high sensitivity to environmental changes. Ideally, the interface does not concern how information is processed at its endpoints such as details of decoding schemes in the wireless node or the internal signaling pathway in cells. In our model, the endpoints of the interface are assumed to process the information and generate signals without error.

Figure 4.2 illustrates a simple two-way interface between a wireless node and a cell. The information flow consists of the following two links:

- *Cell to node*: Cell responses normally alter the state of the surrounding micro-environment. Therefore, a wireless node equipped with a properly designed *bio-sensor* can observe the effect of a cell response in the extracellular environment in a non-invasive fashion. Bio-sensing techniques used to extract the information from bio-signals are beyond the scope of this work, but an extensive body of multidisciplinary research can be found in the literature for interested readers [CM02, Wan05].
- *Node to cell*: To trigger any cell response, the corresponding combination of stimuli should be present. Either propagation of EM signals directly produces a stimulation in the extracellular space, triggering a transduction process, or the cell perceives a secondary effect of the EM signal delivered by auxiliary nano-devices. The possibilities and challenges to create the link from wireless device to biological system

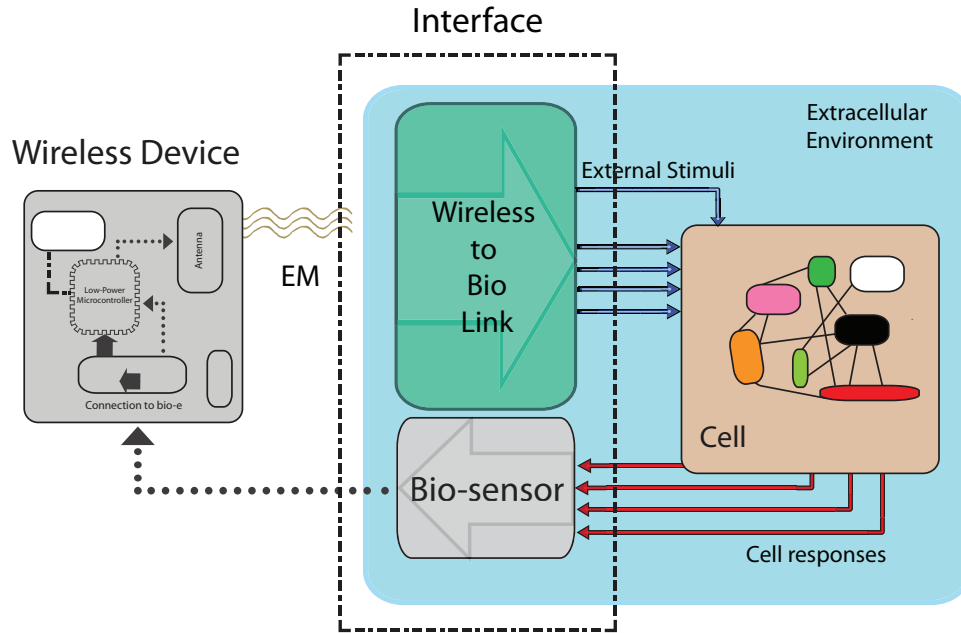


Figure 4.2: The components of a simple interface between a cell and a wireless device.

are the main focus of this part of our research and discussed in detail in the following sections.

The main goal of interfacing mechanism is to convert the message sent by the wireless node in the form of an EM signal to a meaningful set of bio-signals. At the molecular level, EM signals can be seen as series of changes of EM fields in the environment.

4.2.1 Systematic Noise

Biological systems, similar to any communication system, experience systematic noise [Ada91]. Since interactions and signaling in biological systems happen at the molecular level, the energy level of the contributing particles (molecule) nears $k_B T$; hence, the system contains a substantial amount of thermal noise. To ensure a successful activation of the receptor, the energy level of the transduced bio-signals must exceed the threshold level of one or

two order of magnitude greater than the system's thermal noise. The high volume of the noise in the system makes efficient signaling quite challenging.

4.2.2 Signal Transduction

One approach to signal conversion is to use the immediate effect of the wireless signal (i.e. meaningful changes in electric and magnetic fields) as the biological stimulus. Some cell receptors are known to be sensitive to electrochemical voltage variations. For example, ion channels are trans-membrane proteins that control the concentration of a specific ion across the cell membrane by regulating the ion flux. Meaningful changes in an ion concentration such as calcium (Ca^{++}) have been shown to trigger several signaling pathways, and serve as the key mechanism involved in the inter-cellular signaling [NSM⁺05]. For example, the voltage-gated ion channel, which is activated by electrochemical voltage variation, is potentially suitable for interaction with EM signals. The direct use of EM signals as biological stimulation meets the following pair of challenges:

- *Electrical attenuation*: The extracellular fluid is electrically conductive due to the concentration of ions and polar molecules. Therefore, the electric field becomes largely attenuated while propagating in the biological environment [POM10]. In other words, electrical properties of the biological environment channel the energy of the signal to particles other than the target molecule. This forms a two-fold obstacle: reducing the energy of the transduced signal below the detection threshold, as well as creating the possibility of unintended activations elsewhere.
- *Magnetic blindness*: Research has shown that biological systems exhibit limited interactions with magnetic fields due to the absence of magnetic materials [Ada91]. Although natural magnetoreception has been spotted in rare organisms such as magnetotactic bacteria and the migratory birds [KK95], most biological systems lack the natural ability to per-

ceive the magnetic field. However, it is possible to synthetically add a magnetic receptor to the cell. See section 4.3.1 for more details.

A limited number of cell receptors are able to perceive EM fields. In fact, most of the signaling pathways are regulated by chemical, thermal or mechanical stimulation. A more practical approach is to construct a non-EM biological stimulus from the secondary effects of EM signals in biological media. A few possibilities are listed below:

- *Thermal*: It has been shown that high frequency EM fields generate heat while propagating in biological media. Given sufficient amount of time, it may create a temperature increase competent to activate a targeted thermoreceptor [HDMZ06].
- *Mechanical*: Electric and magnetic fields produce mechanical effects (i.e. Force, Torque, etc.) on charged and magnetic materials. Such effects generate a series of motion, vibration, stress, or strain in the cell structure that can be detected by a mechano-sensitive receptor that resides on the cell membrane [Mal74].
- *Chemical*: A combination of thermal and mechanical interactions can be used to release an originally trapped signaling molecule in the extracellular environment, consequently causing the activation of corresponding receptor [HDZ⁺10].

4.3 Enabling Technologies

Efficient and effective implementation of the mechanism mentioned above often requires auxiliary machinery. These nano-scale machines (structures), or simply *bio-devices*, provide the required functionality and compatibility to facilitate the signal conversion in the biological environment. Due to the small size, they can safely attach to biological surfaces or float in the extracellular environment. In this section, we discuss potential enabling technologies that can be integrated, or possibly combined in the design of an efficient and

robust interfacing mechanism. The current state of the technology, challenges, and the improvement possibilities are summarized.

4.3.1 Magnetic Nanoparticles

Magnetic fields, in contrast to electric fields, are not affected by strong attenuation, thus can penetrate deep in biological media and manipulate the targeted magnetic molecules inaccessible to electric signals with the same original energy. Magnetic nanoparticles (MNP), particularly magnetite (Fe_3O_4), among various classes of magnetic materials, make a strong candidate for use in bio-devices due to many attractive characteristics. Small size, in addition to the fact that they can easily be encapsulated in different protein coatings, allows them to attach to virtually all receptors on the cell membrane without undesired consequences on receptors' functionality and cell's health. Most importantly, MNP can easily be manipulated by alternating EM fields (e.g. wireless signals) via *thermal* and *mechanical* effects. While thermal effects of EM exposure on MNPs are well understood and being used in medical procedures such as hyperthermia, details and validity of controlled mechanical interactions of EM fields and MNPs are yet to be fully understood. [KWW10, JSvO⁺09]. Mechanical manipulations of MNPs can be classified based on the use of magnetic *Force* or *Torque*. Since the dimensions of the MNP are often much smaller than the wavelength of the EM signal, the gradient of the magnetic field along the body of the particle is negligible. Therefore, the torque mechanisms, which depend on the amplitude of the field instead of its gradient, are preferable.

Superparamagnetism MNPs with radius of less than 30nm show superparamagnetic behavior, which brings about a number of useful properties. First, such particles show magnetic properties only in the presence of an external field; thus improving the transparency of the interfacing process to the cell in offline mode. Also, the magnetic characteristics of such particles

are function of frequency (i.e. AC susceptibility), which permits the greatly desired frequency multiplexing.

Several mechanisms have been proposed to provoke controlled motion on MNPs using EM fields in a *biological setting* [JSvO⁺09, WKK⁺04, Kir92]. The key disadvantage of such mechanisms is the lack of efficiency since the majority of the energy is dissipated in the process. Accordingly, the wireless device must transmit a huge amount of energy to generate a detectable mechanical stimulus. One possible solution is to create a resonance between the EM signal and the MNP. Resonant systems are known to exchange energy exclusively and efficiently. However, the high viscosity of the extracellular fluid, which is up to 100 times greater than water, promotes highly dissipative mechanical motions; hence, oscillations are mainly over-damped as a result of the large drag forces on the moving particles.

4.3.2 Non-radiative Energy Transfer Mechanisms

Electromagnetic Radiation Dilemma During Electro-Magnetic Radiation (EMR), energy is transmitted as electro-magnetic waves. For a plane wave of a fixed frequency, the power density of the wave is given by its *poynting vector*,

$$\mathbf{S} = \frac{1}{\mu_0} \mathbf{E} \times \mathbf{B} \quad (4.1)$$

Also, the time-averaged magnitude of the poynting vector is

$$\langle S \rangle = \frac{E_0^2}{2\mu_0 c} \text{ W/m}^2 \quad (4.2)$$

Where E_0 and c are maximum amplitude of the electric field and speed of light, respectively. Accordingly, the maximum amplitude of the electric and magnetic fields at distance R from an omnidirectional antenna transmitting at P watts is,

$$E_0 = \sqrt{\frac{\mu_0 c P}{2\pi R^2}} = \sqrt{\frac{60P}{R^2}} \quad (4.3)$$

$$B_0 = \frac{E_0}{c} = \frac{\sqrt{60P}}{Rc} \quad (4.4)$$

Therefore, at the distance of 10 cm, a 1W wireless transmitter generates a surprisingly small magnetic field of intensity $B = 2.58 \times 10^{-7} \approx 0.26 \mu\text{T}$, which is almost 100 times weaker than average magnetic field of the Earth (30–60 μT). The effect of such a small field on nano-scale magnetic particles is infinitesimal. This critically challenges the feasibility of signal conversion for the electromagnetic wave (i.e. radiative EM signal). In contrast, strong alternating magnetic field can be generated simply by physically rotating, or feeding an alternating current (AC) to an electromagnet. In this case, the interaction of magnetic particles and the field is not radiative, and the energy transfer falls in *near-field* category [Yag86].

New paradigms for solar energy conversion, inspired by photosynthesis in leaves, use non-radiative dipole-dipole coupling for direct transfer of energy also called Forster resonance energy transfer (FRET). Jean-Baptiste Perrin showed that energy could be transferred from an excited donor molecule to its neighbors through direct electrodynamic interactions. These near-field interactions would allow the donor to transfer the excitation energy without the emission of a real photon (i.e. radiation). Perrin’s model, however, was based on dye molecules with precisely defined oscillator frequencies, and it incorrectly predicted that energy transfer could occur over distances of up to the visible spectrum wave length ($\sim 500\text{nm}$). In contrast to the earlier assumptions made by Perrin, Forster observed that because the resonance between the oscillating dipoles is not perfect, the energy range of the energy transfer estimated by Perrin must be reduced by a factor of 100 [För48]. This result is in good agreement with experimental FRET observations with standard dyes. As a matter of fact, a similar principle applied to radio waves provides efficient wireless non-radiative energy transfer. *WiTricity* [KKM⁺07, KJS08], based on resonant inducting coupling, demonstrates the transfer of high amount of energy ($\sim 60 \text{ W}$) over a distance of 2m at remarkably high efficiency ($\sim 40\%$). Although the size of the implemented system (coils of radius 40 cm) is a great deal larger than MNP dimensions, the theoretical analysis supports the possibility of similar resonant coupling in nano-scale [KJS08]. It is possible to couple an external resonator to an

engineered nanocoil attached to a targeted receptor, creating an exclusive and efficient channel of energy from outside to the biological system.

4.3.3 Energy Harvesting

Normally, due to limited resources, the transmitted signals from wireless devices contain little amount of energy. This is not the optimal scenario considering that the efficiency of the signal conversion at a passive interface, regardless of signal types, is proportional to the energy level of the incoming signal. A wireless energy harvester unit can be used to accumulate the energy of received EM signals over time and provide a high-energy signal, which can be converted to the desired bio-signal through a simpler and more efficient process.

Chapter 5

Energy Transfer Performance of Electromagnetically-Coupled Mechanical Nanoresonators

We study the energy transfer performance in electrically and magnetically coupled mechanical nanoresonators. Using the resonant scattering theory, we show that magnetically coupled resonators can achieve the same energy transfer performance as for their electrically coupled counterparts or even outperform them within the scale of interest. Magnetic and electric coupling are compared in the *nanotube radio*, a realistic example of a nano-scale mechanical resonator. The energy transfer performance is also discussed for a newly proposed bio-nanoresonator composed of magnetosomes coated with a net of protein fibers.

5.1 Background

Mechanical nanoresonators exhibit resonance behavior involving the mechanical vibrations of the system elements. The natural frequencies of such resonances will, generally, be in the radio frequency range. Nano-scale mechanical resonators coupled with electromagnetic fields have been receiving

significant attention recently [JWGZ07, DPM⁺09, DKPS10]. The ability to interact with electromagnetic fields allow such resonators to be essential parts of nano-scale systems. Imaging, sensing, and targeted actuation in nano-scale are among several emerging technologies that rely on efficient energy and information transfer.

5.1.1 Coupling Types

In principle, nanoresonators may couple to electromagnetic fields by the charge distributions (electric coupling) or by the magnetic moment they carry (magnetic coupling). Traditionally, the energy transfer via electric coupling has received more attention since materials are mostly transparent to the magnetic field. Also, magnetic field intensity in electromagnetic radiations is significantly smaller than the electric field. Consequently, magnetic coupling of mechanical resonators with electromagnetic radiations becomes impractical unless the size of the system significantly decreases. A desirable magnetic coupling, however, can be achieved if the coupling occurs within the near-field range [KJS08]. Take the example of a mechanical nanoresonator operating in a biological environment. In this case, magnetic coupling holds important advantages over electric coupling. First, magnetically coupled systems can provide more *selective* and *localized* energy transfer that is due to the fact that magnetic fields, unlike electric fields, couple weakly with non-targeted surrounding media, which are often not magnetic [KKKDRK92, POM10]. Therefore, magnetic signals suffer from considerably less attenuations while propagating in the surrounding biological media and can drive a targeted resonator inaccessible to electric signals with the same level of energy. In addition, magnetic dipoles are normally more stable than electric dipoles and do not require significant energy from outside to maintain their state.

5.1.2 Our Contribution

This work revisits the interactions of radiofrequency electromagnetic fields with mechanical nanoresonators. In particular, we are interested in the quan-

titative assessment of the energy transfer in such nanoresonators. We use the same methodology presented by Hamam et al. [HKJS07] and focus on low-dissipation conditions that permit resonance. The feasibility of achieving such conditions has been demonstrated in the literature [JWGZ07, SMS⁺01]. The outline of this paper is as follows. We first present a general model for mechanical nanoresonators including electric and magnetic coupling mechanisms and describe the dynamics of the model. Then, we compare the resonant energy transfer performance of the resonator for electric and magnetic coupling using resonant scattering theory. Finally, we sketch a roadmap for a new nanoresonator composed of a magnetite nanoparticle embedded in a net of protein fibers.

5.2 Theoretical Model

In general, the mechanical structure of a nanoresonator consists of an elastic cantilever beam equipped with a specialized tip, which is responsible for electromagnetic interaction, vibrating in a low-viscosity fluid such as low-pressure air. The viscoelastic model of the nanoresonator includes the coefficient of mechanical elasticity, k , and the dissipation coefficient, D . For a cylindrical beam with a spherical tip, $k \cong EI_c/L^3$, where E , I_c , and L are the Young's modulus, second moment of cross-section, and the length of the beam, respectively. Moreover, as shown in [Saz06], the combination of intrinsic (e.g., plastic deformation and surface effects) and extrinsic (e.g., viscous forces of the surrounding fluid) dissipation mechanisms determines the value of D . Because the size of the nanoresonator is much smaller than the wavelength of the external field, the energy transfer is in the form of interactions between the incoming field and dipole moment of the nanoresonator's tip. As shown in Figure 1, we consider two nanoresonators that have identical mechanical structures, yet interact with electromagnetic fields via different coupling mechanisms: electric coupling (\mathfrak{E}) and *magnetic coupling* (\mathfrak{M}). In the case of electric coupling, an alternating current (AC) electric field, $E = E \cos(\omega t)$, produces a force, F , on an electric charge distribution, q , placed at the tip

of the nanoresonator and causes oscillatory deflections in the cantilever. A very similar model has been discussed in the *nanotube radio* [JWGZ07]. For the magnetic coupling, assume the tip of the resonator is made of a ferromagnetic material such as magnetite (Fe_3O_4) and has a magnetic moment of μ . An external magnetic field produces two different motions on such magnetic moment: a translational force produced by the field's gradient and a rotational torque trying to align the magnetic moment with the external field. To produce a translational force that is greater than the thermal noise on a nanoresonator, a magnetic field with ultra-high gradient is required. Producing such magnetic fields drastically increases the complexity of the system; therefore, we choose to neglect the magnetic force and only consider the rotational torque exerted by the external field on the magnetic moment of the nanoresonator's tip. An AC magnetic field, $B = B \cos(\omega t)$, generates a magnetic torque, $\mathcal{T}_m = \mu \times B$, and rotates the tip leading to oscillatory beam deflections. A similar device has been built and used for *ultra-sensitive magnetic resonance force microscopy* [DPM⁺09, SMS⁺01].

The dynamics of the system can be expressed by a Langevin equation for the resonator tip. After linearization for small deflections, we have

$$m\ddot{x} + D\dot{x} + kx = F \cos(\omega t) + N(t), \quad (5.1)$$

where x is the displacement at the tip of the beam; m , the effective mass of the system; and D , the dissipation coefficient. $F = qE$ for electric coupling, while $F = \mathcal{T}/L = \mu B/L$ for magnetic coupling. The term $N(t)$ is a stochastic force with the correlation of $\langle N(t)N(t + \Delta t) \rangle = 2Dk_B T \delta(\Delta t)$, where k_B and T are the Boltzmann constant and temperature in Kelvin, respectively. In the systems we will consider, the amount of energy stored in the resonator is well above $k_B T$. Therefore, we can omit the stochastic term, $N(t)$, from (5.1). The system's natural frequency and the quality factor are given by $\omega_0 = \sqrt{k/m}$ and $Q = \sqrt{km}/D$, respectively. The steady state solution of the system is as follows:

$$x(\omega t) = x_m \cos(\omega t + \varphi), \quad (5.2)$$

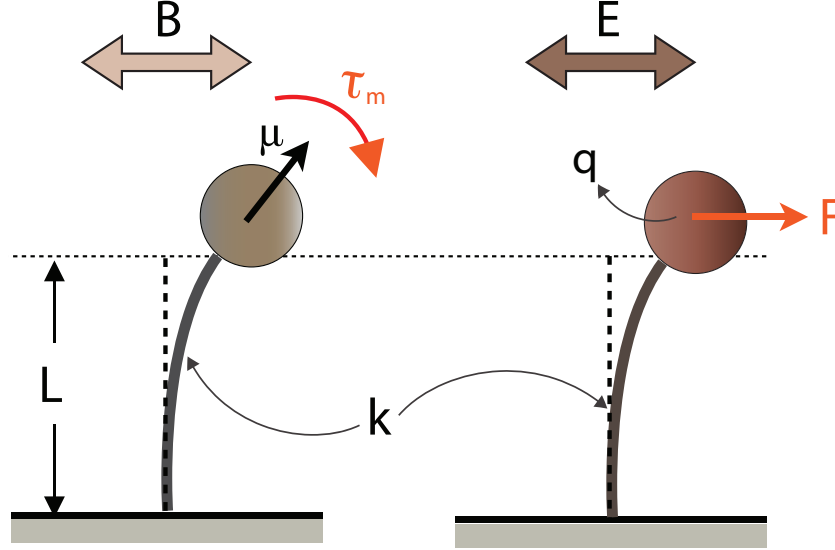


Figure 5.1: An overview of nanoresonators with electric (right) and magnetic (left) coupling. The viscoelastic properties of the resonators are identical.

where x_m and φ are the maximum deflection of the tip and the phase shift, respectively, given by

$$x_m(\omega) = \frac{F/m}{\sqrt{(\omega^2 - \omega_0^2)^2 + (\omega\omega_0/Q)^2}} \quad (5.3)$$

$$\varphi(\omega) = \arctan\left(\frac{\omega\omega_0/Q}{\omega^2 - \omega_0^2}\right). \quad (5.4)$$

A resonance can be achieved if $D < \sqrt{2km}$.

The dynamics of the system can also be expressed by the following Langevin equation for rotational oscillation [JBN11b]:

$$I\ddot{\theta} + C\dot{\theta} + \kappa\theta = \mathcal{T}\cos(\omega t) + \psi(\omega t) \quad (5.5)$$

Here, $\theta = x/L$ is the angular displacement, $I \cong mL^2$ is the system's second moment of inertia, $\kappa \cong kL^2$ is the rotational spring constant of the cantilever,

and ψ is the stochastic torque caused by the thermal noise. For the magnetic coupling, $\mathcal{T} = \mu B$, while $\mathcal{T} = qEL$ in the case of the electric coupling.

5.3 Energy Analysis

We now consider the total energy of the oscillator

$$U = \frac{1}{2}mv^2 + \frac{1}{2}kx^2. \quad (5.6)$$

When $\omega = \omega_0$, this quantity is time-independent and is given by

$$U = \frac{F^2 Q^2}{2k}. \quad (5.7)$$

One can think of U as the energy capacity of the resonator. An important observation is that U scales with Q^2 .

Next, we consider the energy absorbed by the nanoresonator during the relaxation time $\tau = Q/\omega_r$. This quantity can be calculated by averaging the instantaneous power absorbed by the nanoresonator, P , over τ . For our system, P can be written as inner product of incident force and velocity of the resonator

$$P = F \cdot v = F \cos(\omega t) \frac{dx(\omega t)}{dt}. \quad (5.8)$$

Plugging the solution from (5.2) results in

$$\begin{aligned} P &= -F\omega x_m \sin(\omega t + \varphi) \cos(\omega t) \\ &= F\omega x_m \times \frac{(\sin(2\omega t) \cos(\varphi) + (1 + \cos(2\omega t)) \sin(\varphi))}{2} \end{aligned} \quad (5.9)$$

The average of sinusoidal terms in the right hand side of the (5.9) over an integral number of cycles equals zero. After some algebra, the average absorbed power, \bar{P} , is given by

$$\bar{P} = \frac{F\omega x_m \sin(\varphi)}{2}. \quad (5.10)$$

At the resonance frequency, $x_m = FQ/m\omega_r^2$ and $\varphi = \pi/2$, which gives the average absorbed power of $\bar{P} = F^2Q/2m\omega_r$. Thus, the energy deposited in the nanoresonator during the relaxation time τ is

$$\Delta U_r = \bar{P}\tau = \frac{F^2Q^2}{2m\omega_r^2} = \frac{F^2Q^2}{2k}. \quad (5.11)$$

Note that the energy absorbed by the resonator over the relaxation time matches the resonator energy capacity. In general, the calculation of the force (or torque) exerted on the nanoresonator through electromagnetic coupling is not straightforward. As an alternative approach, one can use scattering theory [HKJS07, BW54], which allows to work with fluxes instead of forces, to estimate the energy deposited on the resonant system. The two approaches are equivalent since our theoretical model is solely based on dipole-dipole interactions. In the next section, we will use this more convenient method to study the resonant energy transfer.

5.4 Resonant Scattering Analysis

The coupling between external fields and the nanoresonator consists of an absorption and a scattering process. According to the scattering theory, the power absorbed by the resonant system equals to $P_a = \Phi\sigma_a$, where Φ is the incident electromagnetic power flux, and σ_a is the absorption cross-section given by [HKJS07, BW54]

$$\sigma_a(\omega) = 12\pi\left(\frac{c}{\omega}\right)^2 \frac{\Gamma_a\Gamma_s}{(\omega - \omega_r)^2 + (\Gamma_a + \Gamma_s)^2/4}. \quad (5.12)$$

Here, c is the speed of light; Γ_a , the absorption width; and Γ_s , the scattering width. The widths are the ratio of the power loss to the characteristic energy of the corresponding process. For process i , $\Gamma_i = 1/\tau_i = \omega/Q_i$, where τ_i and Q_i represent the relaxation time and the quality factor, respectively. The total energy absorbed by the resonant system during the resonant process is given by the following:

$$\Delta U(\omega) = P_a(\omega) \times \tau_a = \frac{\Phi\sigma_a(\omega)}{\Gamma}, \quad (5.13)$$

where $\Gamma = \Gamma_a + \Gamma_s$ is the total width of the system. For nano-scale systems of interest, $\Gamma \approx \Gamma_a$ because $\Gamma_s \ll \Gamma_a$. The maximal energy transfer occurs at the resonant frequency and can be written as

$$\Delta U_r = \frac{48\Phi c^2}{\omega_r^2} \left(\frac{\Gamma_s}{\Gamma_a^2} \right) = \frac{48\Phi c^2}{\omega_r^4} \Gamma_s Q_a^2. \quad (5.14)$$

Q_a is obtained from the steady state solution.

By definition, the width of the scattering process is equal to the inverse of the decay time of radiating dipole given by the following:

$$\Gamma_s = -\frac{d \ln U(t)}{dt} = -\frac{dU/dt}{U} \quad (5.15)$$

where U is the energy of the resonator, and $P_r = dU/dt$ is the radiative power of the resonator's dipole. For the electric dipole model (E), we have

$$P_r^E = -\frac{1}{4\pi\epsilon_0} \frac{p_0^2 \omega^4}{3c^3} \quad (5.16)$$

$$U^E = \frac{1}{2} k x_m^2, \quad (5.17)$$

where $p_0 = qx_m$ is the maximal amplitude for the electric moment of the resonator. Thus, one obtains the following scattering width for the system:

$$\Gamma_s^E = \frac{q^2}{4\pi\epsilon_0} \frac{2\omega^4}{3c^3 k}. \quad (5.18)$$

Replacing (5.18) in (5.14) results in

$$\Delta U_r^E = \frac{q^2}{4\pi\epsilon_0} \frac{32\Phi Q_a^2}{ck}, \quad (5.19)$$

which confirms that the energy deposited scales as Q^2/k .

Using classical electrodynamics [Jac67], one can show that the radiative power of an oscillating magnetic dipole of moment μ_{eff} is given by replacing p_0 by μ_{eff}/c in (5.16). In the case of the spherical MNP shown in Figure 1, if θ_m is the maximum angular deflection, then the oscillating part of the magnetic dipole of moment is $\mu_{\text{eff}} = \mu \sin^2(\theta_m)$. Therefore, for the

magnetic coupling model (\mathfrak{M}), one can follow the same derivation as in the electric coupling scheme (\mathfrak{E}) and obtain

$$P_r^{\mathfrak{M}} = -\frac{1}{4\pi\epsilon_0} \frac{\mu^2 \omega^4 \theta_m^2}{3c^5}, \quad (5.20)$$

$$U^{\mathfrak{M}} = \frac{1}{2} \kappa \theta_m^2 = \frac{1}{2} k L^2 \theta_m^2. \quad (5.21)$$

Therefore, the corresponding radiation width and deposited energy are

$$\Gamma_s^{\mathfrak{M}} = \frac{\mu^2}{4\pi\epsilon_0} \frac{2\omega^4}{3c^3 k (Lc)^2} \quad (5.22)$$

$$\Delta U_r^{\mathfrak{M}} = \frac{\mu^2}{4\pi\epsilon_0} \left[\frac{1}{Lc} \right]^2 \frac{32\Phi Q_a^2}{ck}. \quad (5.23)$$

Note that Q_a and k in Equations (5.19) and (5.23) only depend on the viscoelastic structure of the resonator and are independent from the coupling type (magnetic or electric). Given a similar viscoelastic structure, the energy absorption value for electric and magnetic coupling will be comparable if $\mu/Lc \approx q$. For nano-scale systems of interest, the condition $Lc < 1,000 \text{ m}^2/\text{s}$ normally holds. By comparing (5.23) to (5.11), it is possible to derive an expression for the average magnetic force experienced by the nanoresonator over the resonance relaxation time, which is given by

$$\bar{F} = \sqrt{\frac{\mu^2}{4\pi\epsilon_0} \frac{32\Phi}{c^3}}. \quad (5.24)$$

5.5 Applications

Having discussed the mechanical dynamics of the nanoresonator as well as the theoretical formulation for energy transfer performance of different coupling mechanism, we apply our analysis to a possible nanoresonator sketched in Figure 2, and we also discuss the feasibility of a bio-nanoresonator composed of protein coated Fe_3O_4 nanoparticles.

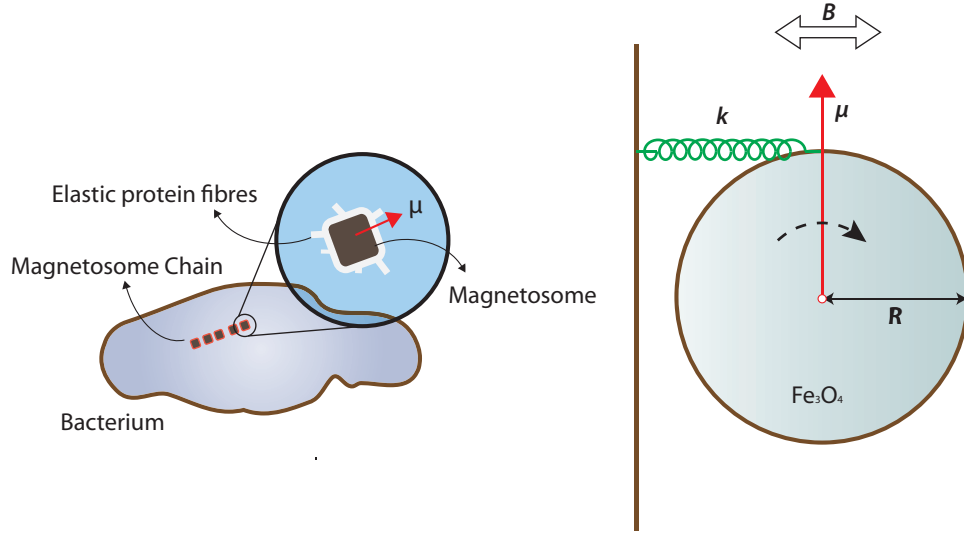


Figure 5.2: Magnetosome arrangement in magnetotactic bacteria. The magnified part shows how elastic protein fibres embed magnetite (Fe_3O_4) crystals in the cytoskeleton. Interaction of the magnetic dipole of the crystal with external fields within its viscoelastic environment can be analyzed by our presented theoretical model as a torsional nanoresonator shown on right hand side. Magnetic torque rotates the MNP around its center of mass. The rotational spring constant is given by $\kappa = kR$, where k is the aggregate rigidity of the connecting protein fibers and R is the radius of the MNP. Since the Reynold number of the MNP is very small, the drag forces are given by Stoke's law. Therefore, the rotational damping coefficient is $C = 6\pi\eta R^3$, where η is viscosity of the surrounding fluid.

5.5.1 Replacing Magnetic Coupling in Nanotube Radio

In our first example, we compare the energy transfer performance of the magnetic and electric coupling in the nanotube radio, a realistic example of a mechanical nanoresonator [JWGZ07]. We replace the electric dipole of the nanotube tip with a magnetic dipole in the form of spherical magnetite nanoparticle. According to the original study, a nanotube radio built from a cylindrical carbon nanotube of length $L \approx 1 \mu\text{m}$ holding a net charge of $q = 200 e^-$ absorbs an amount of energy enough to detect radio signals from the electromagnetic radiation. To achieve the same amount of energy

deposit, the magnetic moment of the replacement tip should be in the order of $\mu \approx qLc = 9.6 \times 10^{-15} \text{ Am}^2$, which can be obtained by placing a magnetite nanoparticle of radius R approximately 160 nm.

5.5.2 A Functional Mechanical Nanoresonator in Biological Setting

Another interesting application is the possibility of transmitting energy to magnetic nanoparticles in the biological setting. Biogenic magnetite nanoparticles called magnetosomes, first discovered in magnetotactic bacteria [Bla75], are also found in the brain of many animals and are believed to participate in determining the orientation in several species such as migratory birds [KWW10]. Interestingly, magnetosomes consist of magnetite particles of radius 50 to 100 nm and are embedded in the cytoskeleton bound to a viscoelastic system formed by a net of protein fibers. Because magnetic nanoparticles of such size are single domain with high coercivity [MW09, HDMZ06], the magnetosome can be represented as a torsional nanoresonator with magnetic coupling (see Figure 2).

The magnified part in Figure 5.2 shows how elastic protein fibers embed magnetite (Fe_3O_4) crystals in the cytoskeleton. Interaction of the magnetic dipole of the crystal with external fields within its viscoelastic environment can be analyzed by our presented theoretical model as a torsional nanoresonator shown on the right hand side. Magnetic torque rotates the MNP around its center of mass. The rotational spring constant is given by $\kappa = kR$, where k is the aggregate rigidity of the connecting protein fibers, and R is the radius of the MNP. Since the Reynold number of the MNP is very small, the drag forces are given by Stokes' law. Therefore, the rotational damping coefficient is $C = 6\pi\eta R^3$, where η is the viscosity of the surrounding fluid.

According to Winklhofer and Kirschvink [WK10], the rigidity of the cytoskeleton can be estimated by $\kappa = 100 k_B T / \text{Rad}$ per connecting filament. Thus, for magnetite particles with a density of $\rho = 5,200 \text{ Kg/m}^3$, a radius of $R = 100 \text{ nm}$, and the number of the connecting filaments ranging from 1 to 1,000, the natural frequency of the oscillator will fall between 2 and 66 MHz.

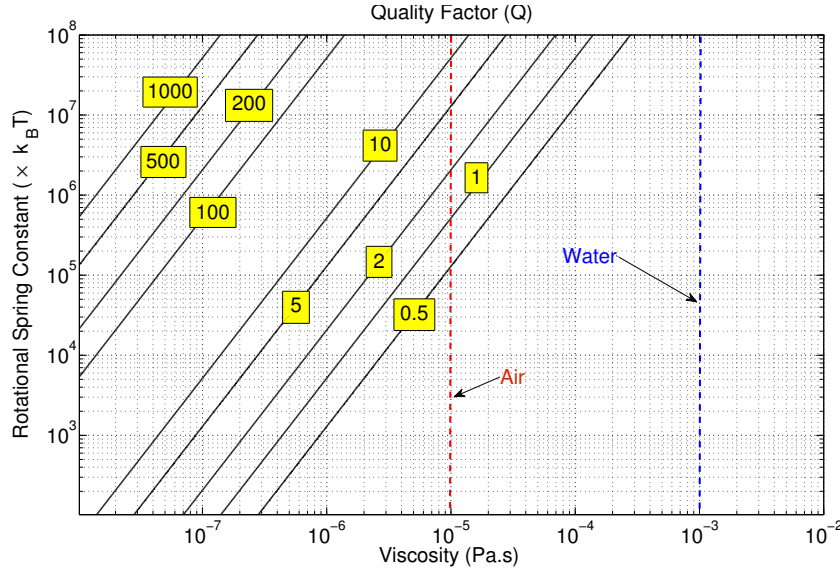


Figure 5.3: (Color online) Quality factor of the resonance for reasonable range of values for the environment viscosity and the rotational spring constant of elastic environment (in terms of $k_B T$). We assume the design includes a magnetite nanoparticle of Radius 100 nm. Note that resonance is possible in the region above $Q = 0.5$ line. It is shown how resonance of a given quality can be achieved in lower frequency by reducing the viscosity experienced by the resonator.

A resonance is in principle not possible if we adopt the standard viscosity of the cytoplasm [Ada02]. However, in a carefully engineered synthetic system, one could lower the drag forces in order to achieve resonance and higher quality factor up to $Q = 100$. Figure 3 shows possible quality factor values for a nanoparticle of radius 100 nm, assuming that the viscosity and elastic constants could be controlled.

Technologies to Reduce the Drag Forces In order to achieve higher quality factor, the nanoresonator should experience smaller viscous resistance. For instance, one can reduce drag forces in the system by coating the magnetite nanoparticle with hydrophobic proteins or lipids. In this case, the hydrophobic coat acts as a lubricant [PF95, SYF⁺08]. In a more sophisticated design, a

multi-layer shell of hydrophobic proteins may be used to engulf the nanoresonator and repel water molecules [HCW⁺12]. In order to aggressively reduce the rotational friction, the nanoresonator could be packed in an inorganic shell that completely excludes the system from the cytoplasm. The elastic protein fibers may be replaced by synthetic nanowires or nanotubes with carefully designed rigidity. For example, del Barco et al. [BAZ⁺01] have demonstrated the possibility to have free rotation of magnetic nanoparticle embedded in a solid matrix.

Assuming that high quality factor, $Q = 100$, can be achieved, one finds that an AC magnetic field of intensity $B = 3.5$ mT, generating an electromagnetic flux of 10 W/m², deposits a significant amount of energy $\Delta U = 2,500 k_B T$ into the system over the resonance relaxation time. Since this field intensity is well below the coercivity field of the nanoparticle [HDMZ06, MW09], we neglect the energy losses via magnetic reversal. If this energy was entirely manifested as heat, the temperature of the magnetosome would be increased by 0.5°C during the relaxation time $\tau = 0.1 \mu\text{s}$. As shown in Figure 3, $Q = 10$ corresponds to $\omega_0 = 66$ MHz, in air ($\eta = 10^{-5}$ Pa.s), while the same quality factor can be achieved at frequencies as low as about 1 MHz if the viscosity can be reduced by a factor of 100 compared to air. Magnetically coupled mechanical nanoresonators with high quality factor show good energy transfer performance while being tunable and may be useful in frequency selective heat production in the biological environment. The important contribution of mechanical motions in magnetic hypothermia has been experimentally shown in [AFR⁺11]; however, these applications have not yet benefited from the resonant energy transfer since their quality factors are well below one.

5.5.3 A Carbon Nanotube based Nanoresonator in Biological Setting

In this section, we propose a design for a passive nano-scale wireless receiver that can operate in a viscous bio-material and that can be tuned within a wide range of radio frequencies (100s MHz - few GHz). The receiver is composed of an integrated magnetic nanoparticle with a carbon nanotube. We show

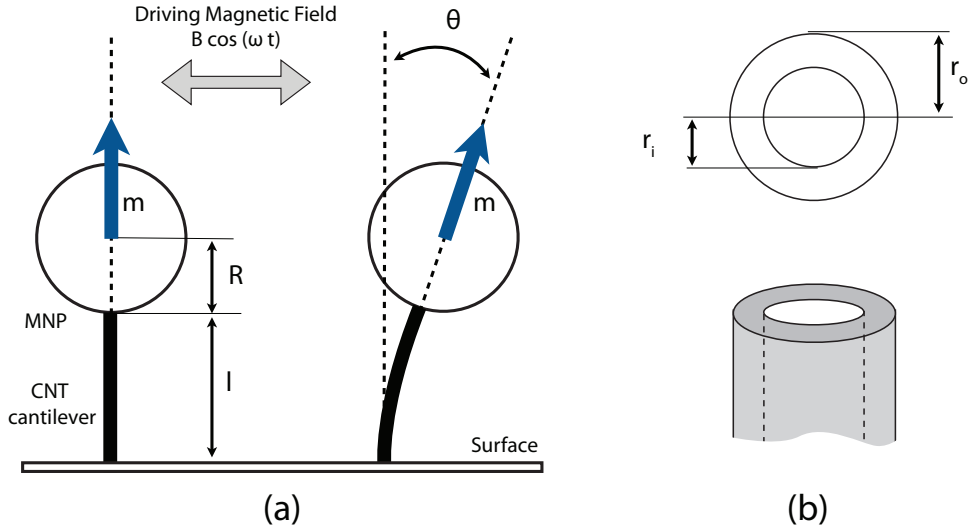


Figure 5.4: The illustration of the system. (a) an overview of the components of the mechanical nanoresonator at initial (Left) and operating (Right) conditions. Dimensions and angles used in the theoretical analysis are shown. (b) Cross section of the carbon nanotube cantilever.

through theoretical analysis that such a receiver can effectively resonate with radio frequency signals and efficiently transduce the high frequency magnetic torque into actuation (e.g., 100nm carbon nanotube bound to 100nm magnetic nanoparticle can resonate at ~ 150 MHz). This is made possible thanks to advances in the manufacturing of carbon-nanotubes and magnetic nanoparticles. Tunable resonance at high frequency is the key in enabling multiplexed interactions and more sophisticated targeted actuations.

As shown in Figure 5.4, the multi-wall carbon nanotube (MWCNT) cantilever is clamped to the surface, and firmly attached to a spherical magnetic nanoparticle (MNP) on the free end. Following our theoretical model, an alternating external magnetic field exerts a magnetic torque on the MNP creating an elastic deflection in the CNT.

We derive the equations for I , C , k , and τ_m for the presented resonator by computing the torques and moments of inertia with respect to the cantilever's

base. External electromagnetic torque is given by

$$\tau_m = \mu \times B = \mu B \sin(\pi/2 - \theta) \cos \omega t \quad (5.25)$$

$$\begin{aligned} &= \mu B \cos \theta \cos \omega t \\ &= \mu B \cos \omega t. \end{aligned} \quad (5.26)$$

Neglecting the mass of the cantilever, the moment of inertia of the system equals the moment of inertia for a spherical mass (i.e. the MNP) with respect to cantilever's base, and is given by

$$I = \frac{2}{5}mR^2 + mD^2, \quad (5.27)$$

where m is the mass of the MNP, and $D = (l + R)$ is the distance of MNP's center of mass from the base. Therefore,

$$I = m\left(\frac{2}{5}R^2 + D^2\right) \quad (5.28)$$

$$= \frac{4\pi}{3}\rho R^3\left(\frac{2}{5}R^2 + (l + R)^2\right), \quad (5.29)$$

where ρ is the density of the magnetite.

The elasticity coefficient (i.e. equivalent spring constant) for a cantilever beam is given by Bernoulli-Euler equation. For small deflections of the beam with a torque load at the tip, we have

$$k = \frac{EI_c}{l}, \quad (5.30)$$

where E , I_c , and l are Young's modulus, second moment of cross-section, and length of the beam [Mei01]. MWCNT is basically a cylinder, thus

$$I_c = \frac{\pi}{4} (r_o^4 - r_i^4), \quad (5.31)$$

where r_o and r_i are outer and inner radii of the CNT.

Dissipation Mechanisms Several dissipation mechanisms may affect the oscillations of the resonator. The dissipations in nanoresonators can be

divided into two categories: a) *Intrinsic losses*, which are due to imperfections and interactions within the structure of the resonator (e.g. phonon-phonon interactions, thermoelastic effect). b) *Extrinsic losses*, which are the result of interactions with the surrounding environment (e.g. viscous friction, clamping losses). In this model, we only consider the extrinsic dissipations. The viscous nature of the biological media makes the viscous friction the dominant factor among the extrinsic losses. For the sake of simplicity in this paper, we only consider dissipations due to drag forces in the fluid. Small particles such as nanoresonator components have very small Reynolds number ($R_e \rightarrow 0$), thus fluid behaviour follows the Stokes' law. For a spherical object of radius R in this condition we have,

$$F_D = 6\pi R\eta v, \quad (5.32)$$

where η and v are fluid viscosity and velocity of the object. Substituting for $v = (l + R)\dot{\theta}$, and $C = \tau_D/\dot{\theta}$, we have

$$\begin{aligned} C &= \frac{\tau_D}{\dot{\theta}} = \frac{F_D \times (l + R)}{\dot{\theta}} \\ &= 6\pi R\eta(l + R)^2. \end{aligned} \quad (5.33)$$

Note that because of the small moving area, the drag forces on the cantilever are negligible and not considered.

Substituting from Eq. 5.29, 5.30, and 5.33 results in the expanded form of resonance condition below:

$$54\eta^2(l + R)^4 < E\rho R\left(\frac{2}{5}R^2 + (l + R)^2\right)(r_o^4 - r_i^4). \quad (5.34)$$

5.5.3.1 Design and Optimization

Having explored the theoretical model for the system, this section discusses the design and optimization of the system. The goal is to design and to optimize a resonator that operates at a given resonant frequency in a given microenvironment. Identifying the key parameters of the design is necessary to achieve the desired performance. The equations derived in the preceding

section include two different types of parameters. First are the *material properties*, which include Young's modulus (E), density (ρ), and viscosity of the microenvironment (η). Second are *structural parameters*, which are MNP radius (R), CNT length (l), and radii (r_o and r_i). Adjusting the material properties could potentially require radical changes in the design and setup and might not be possible at all. In contrast, structural parameters provide much wider range of flexibility, thus make good tuning parameters for the resonator.

A numerical example for design and optimization of a real world system is presented below. Note that in this example R and l serve as tuning parameters and the rest of the parameters are given as follows: MNP is made of magnetite (Fe_3O_4) with density of $\rho = 5200 \text{ Kg/m}^3$. The cantilever beam is a carbon nanotube with Young's modulus of $E = 5 \text{ TPa}$, and outer and inner radii of $r_o = 5 \text{ nm}$, $r_i = 2 \text{ nm}$, respectively. The system will be installed in an aqueous environment, therefore $\eta = 10^{-3} \text{ Pa.s}$. Finally, the overall size of the system should stay within reasonable range for biological application (i.e. less than few micrometers).

We first look at the possibility of the resonance for such a system. The resonance happens provided that the inequality presented in Eq. 5.34 is fulfilled. Fig. 5.5 shows the resonant frequency and quality factor for the system for reasonable values of R and l . Data from Fig. 5.5 suggests that resonant conditions are achievable for a large range of tuning parameters (Colored region).

The next step is to find the optimal configuration (or an optimal set of configurations) in which the resonator operates at desired resonant frequency. This is possible by determining the cross section of the graph of resonant frequency as a function of R and l at given frequency. Operating at a frequency is not possible if the cross section is empty. Otherwise, each point on the cross section represents a valid configuration in which the resonator operates at the desired frequency. Fig 5.6 illustrates this process for our numerical example. As shown on the graph, $(R = 100\text{nm}, l = 42\text{nm})$ configuration leads to resonant frequency of $f_r = 50 \text{ MHz}$, while $f_r = 300 \text{ MHz}$ can be achieved

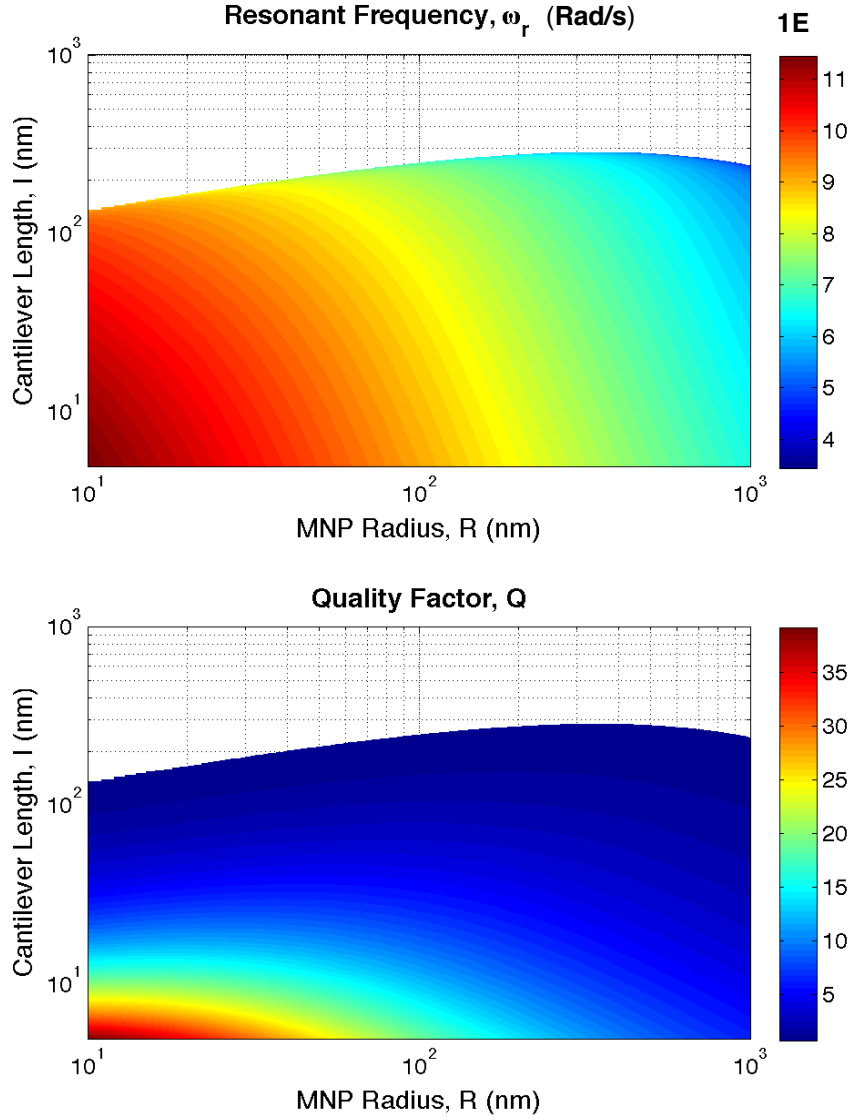


Figure 5.5: (Color online) Resonant frequency ω_r (upper graph) and Quality factor (lower graph) for reasonable range of values for MNP radius ($10 \text{ nm} < R < \mu\text{m}$) and CNT length ($5 \text{ nm} < l < \mu\text{m}$). The points located outside the colored region represent overdamped oscillations. Graphs are generated in MATLAB.

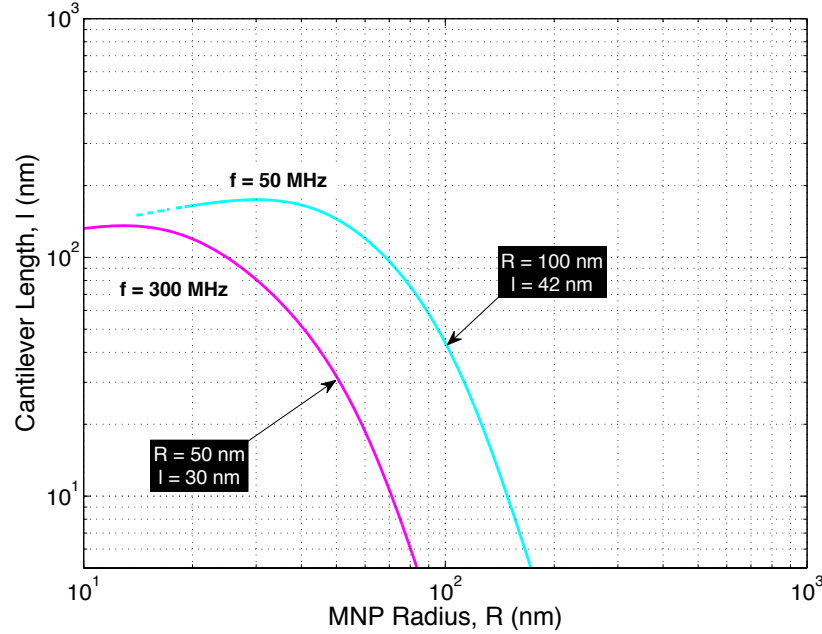


Figure 5.6: (Color online) Optimization look-up graph for a magnetite/(5,2)-CNT resonator operating in water at 60 MHz (blue line) and 300 MHz (purple). Any point on an specific frequency line is a valid configuration for R and l , which results in a resonator with resonant frequency of the line's nominal frequency. Graph is generated in MATLAB.

by choosing ($R = 50\text{nm}$, $l = 30\text{nm}$). These are reasonable values in today's manufacturing technology.

5.5.3.2 Discussion

The tiny size of nanoresonators significantly limits their amount of energy. With such limited energy budget, overcoming the ambient thermal noise (i.e. $k_B T$, where k_B is the Boltzmann constant and T is the temperature in Kelvin.) becomes a challenging obstacle. In order to have a meaningful impact on the surrounding microenvironment, the total energy of the resonator must exceed $k_B T$. This determines the *sensitivity* of the resonator to external actuations.

Another important challenge is the mechanism by which the CNT is at-

tached to the MNP. A very strong (covalent) bond is required to achieve good performance. While the process of attaching an MNP to a CNT is still underexplored, recent research demonstrates manufacturing similar bonds by chemically modifying the surface of MNPs and CNTs [CNB⁺07].

Finally, even in the case of good coupling between the nanoresonator and the external field, the oscillations eventually become non-linear. This makes the design that is only based on linear resonance flawed and not sufficient. In this work, we skipped the non-linear analysis due to the limited space.

5.6 Conclusive Remarks

In conclusion, we have shown that carefully engineered magnetically coupled nanoresonators can match the energy transfer performance of its electrically coupled counterpart, while providing a more selective and robust interaction in biological environments. We have used a unifying framework of resonant energy transfer for electrically coupled and magnetically coupled mechanical nanoresonators and compared the performance for the two couplings. Our analysis suggests that if the interacting electric dipole of a small electrically coupled resonator is replaced by a magnetic dipole, a comparable amount of energy can still be deposited on the system. We have considered the example of nanotube radio, and we have shown that the strength of electromagnetic coupling remains the same using a magnetite nanoparticle of radius 160 nm instead of the charged tip. We have proposed a new resonator composed of magnetosomes embedded in a net of protein fibers and analyzed its energy transfer performance. We have discussed possible pathways to further improve the quality factor of the resonator. While this article focuses on quantitative aspect of energy transfer, our work also opens up new interesting questions on how to use efficient energy channels to transmit information to a nano-scale device or organism. Characterizing the transmission of information and the channel capacity [Sid09] will be discussed in future studies.

Chapter 6

Related Work

6.1 Passively-powered Wireless Systems

6.1.1 Radio Frequency Identification (RFID)

RFID tags have the potential to deliver information anytime, anywhere [Wei05, EPC08]. However, RFID tags have significant limitations making them impractical for delivering a substantial amount of information to commodity smartphones. First of all, equipping smartphones with an RFID reader is a significant and challenging modification to the phone hardware. Secondly, among the three types of RFIDs (i.e., passive, active, and semi-active), only the passive ones do not require a battery and therefore satisfy severe longevity constraints. However, passive RFIDs require the readers to transmit at high power (in the order of watts), with large antennas. Furthermore, such RFIDs are only capable of storing a very limited amount of information (e.g., 128 bytes) and are not capable of sophisticated interactions.

6.1.2 WISP

Several RF-energy harvesting techniques and prototypes were explored over the last few years. The WISP platform and its variants harvest energy from RFID reader [SYP⁺08] and TV radio stations [BPS⁺08], and are capable of

powering a ultralow-power microcontroller. The WISP was also used as a batteryless sensor node to communicate with a traditional RFID reader [SYP⁺08]. It relies on a high energy sources (30dBm) operating at a medium RF frequency (915MHz). The constraint of the iPoint to operate on the low RF energy from smartphones (few dBm) and higher WiFi frequency (i.e., 2.4GHz) requires more advanced RF-energy harvesting mechanisms that we present in the next sections. Other platforms for wireless power transfer exist but require either high transmission power on the 915MHz band [pow], or require highly customized transmitters and receivers such as in wireless power transfer via strongly coupled magnetic resonances [KKM⁺07].

6.1.3 Near-Field Communication (NFC)

The Near-field Communication (NFC) [nfc], founded by Nokia, Phillips and Sony in 2004, is a set of standards based on RFID technology that allows devices such as smartphones to establish a communication. Communications take place at 13.56 MHz over very short range of less than few centimeters, which typically involves two devices touching each other. NFC allows several modes of communications including communication with a passive device. The communication scheme is ASK with Miller or Manchester coding. Data rate varies between 106 and 424 kbit/s. Because of the very simple and fast set-up, NFC can be used to initialize more sophisticated wireless communication to start peer-to-peer networking. The energy transfer mechanism is based on electrodynamic induction between two loop antennas. In comparison to solution presented in this work, NFC exchanges data at higher data rates, but operates at shorter ranges. Also, NFC functionality on a smartphone requires additional designated hardware.

6.1.4 Bokode

Recently, a clever alternative solution to RFID tags and traditional barcodes, called bokode, was developed to deliver information from a dot of 3 millimeters diameter encapsulating a high density Data Matrix code [MWH⁺09].

The information is revealed by putting an off-the-shelf camera in an out of focus mode. This solution has the advantage to reduce the size of the tag and increase the information density but still keeping the tag passive. However, bokode still lacks a two-way communication capability and requires sophisticated digital cameras (10Megapixel with a large lens) with in/out focus capability. In the future, if smartphones become equipped with controllable focus cameras, the envisioned iPoint system might benefit from integrating a bokode-based LCD display to deliver information to a smartphone at a lower energy cost.

6.1.5 Microwave Power Transmission

A mechanism based on RF energy harvesting has been explored to transfer huge amount of energy over very long distances[MM02, YC92]. For example, high-power directional antennas have been used to transmit energy to satellites from earth. The rectennas with efficiencies up to 95% have been demonstrated [TKT⁺12].

6.1.6 Resonant Inductive Coupling

Non-resonant inductive coupling, which is being widely used in transformers, suffers from stiff drop in efficiency when distance between interacting coils increases. Karalis et al. [KKM⁺07] have shown that extremely high efficiency over mid-range can be achieved if the inductive coils couple in their resonant frequency. They have built a system that can transfer 60W of power over distances up to 2 meters with 90% efficiency. Their work is the basis for a commercial technology called WiTricity [Ano] that promises efficient wireless power transfer that can be used to wirelessly power electronic devices within environments such as home or office. Several methods based on resonant inductive coupling have been proposed for wireless energy transfer in the biological setting, for instance to power medical implants in body [Poo09, RL12].

6.2 Remote Control of Biological Systems

While fully operational bio-enabled wireless devices are still a research dream, progress in several fields is making their components more plausible. Recent research has shown that it is possible to manipulate and control cell function, in vitro and in vivo, with an external magnetic field [Dob08, HHD05, GFM95, HH88, HDZ⁺10, MAR⁺00, HMDH08, Rab02, KRU⁺09]. This is achieved by binding Magnetic Nano-Particles (MNP) to the surface of cells, and applying a static magnetic field to either twist (torque) or pull the MNP. Huang et al. [HDZ⁺10] demonstrate the use of high-frequency magnetic field to heat up the magnetic nanoparticles attached to temperature-sensitive receptors in live C-elegans worms, controlling the behavior of the organism. An FM/AM controlled cell excitation was also shown to propagate through from cell to cell as inter-cellular Ca^{2+} waves [Ber97]. Other researchers have shown that it is possible to down-convert an RF signal to a very-low frequency torque of a magnetic nano-particle ($\sim 3\text{Hz}$) [JSvO⁺09]. Recently, it has been shown that some cellular components such as structural microtubules may be excited with external electromagnetic radiation [Cif12]. The resonance frequency of microtubule structure have been estimated [HCK⁺11].

6.2.1 Molecular computing and communication

The computer and networking community have been investigating various molecular computing and communications paradigms obtaining theoretical results, defining frameworks, and designing novel mechanisms for bio-enabled communications [SCWB08, NSK⁺08, NSM⁺05, JNN09].

6.2.2 Synthetic Biology

The synthetic biology community has been making steady progress on designing, programming and standardizing biological systems [SEK08]. For example, a class of stochastic chemical reaction networks was recently shown to be Turing universal and can therefore compute any computable function. Digital

memory biological devices were successfully designed from transcriptional networks. Biological bi-stable switches were also successfully engineered.

6.2.3 Extremophiles

Finally, progress has been made in understanding extremophile bio-organisms, which thrive in extreme environments from -273°C to $+151^{\circ}\text{C}$, tolerate over 1,000 times more radiation than other organisms [ZSB⁺06], and can be used as a chassis for synthetic biology.

Chapter 7

Conclusion and Future Research Directions

Energy efficiency of wireless communications has remained a key obstacle that greatly influences the overall performance of wireless networks. Critical dependency of wireless devices on their limited source of energy requires careful adjustments in computations and communication to conserve as much energy as possible. In some particular applications of wireless communication, the energy conservation issue becomes so severe that having a local source of energy (battery) is not practical or feasible. The first example is wireless sensor networks in which the sensor node consumes a vast majority of its energy on keeping its wireless radio on waiting for a typically rare incoming message. The second example of severe energy deficiency emerges when the size of the receiver is reduced, most notably in miniaturized wireless devices designed to operate at very small scales.

In this thesis, we have studied the wireless transfer of energy alongside information as a solution to energy conserving problem in the aforementioned scenarios. We categorized our work into the following two studies:

First, We have presented the notion of consolidated energy and information channel for wireless sensor networks. We have argued that energy conservation issue at the receiver side can be eliminated by transferring en-

ergy via wireless signals. We have reviewed the steps required to enable such functionality in wireless sensor networks, studied potential wireless energy transfer methods, and presented the necessary modifications to wireless communication after the integration of energy transfer. We have introduced iPoint, a passively-powered wireless device that is capable of communicating with a commodity smartphone without any need for a battery or any specific hardware modification on the phone. The complete design and optimization of the software and hardware of the device were presented. We presented two new communication schemes: Packet length modulation (PLM) and LCD Pattern Coding (LPC). We provided the theoretical performance analysis, and also performed a rigorous experimental evaluation of the system. iPoint is an example of a wireless device that consumes no energy unless it is necessary. At first glance, this seems similar to the functionality of RFID passive tags. However, iPoint's ability to communicate with a device as common as a smartphone without any hardware modification (just by installing an application) makes the information much more accessible. The design of the passively-powered devices is a vastly complex problem. While we tried to optimize the different components of the design as much as possible, there is still room for improvement. In the future research, it would be interesting to consider more sophisticated antenna designs to improve the energy harvesting performance. Another interesting problem is to study the effects of installing security schemes on top of the presented communication protocols on the overall energy efficiency of the system.

In the second study, we have looked into small-scale wireless communication, particularly in biological settings. We have introduced bio-enabled wireless networks that interface wireless communication with biological systems. The immediate benefits of extending the scope of the wireless communication is twofold: It enables remote control of biological systems, with several potentials in nanomedicine. On the other hand, it makes leveraging the evolution-perfected prowess of biological organisms (extreme energy efficiency, robustness, self-assembly, to name a few) into the computations and communications. Building such an interface between these two seem-

ingly different worlds requires nano-scale auxiliary machinery that we call bio-devices. Due to their extremely small size, bio-devices cannot have an energy source, therefore energy has to be deposited from outside. We have conducted a theoretical study to quantitatively assess the energy transfer performance of magnetically-coupled mechanical nanoresonators, that can efficiently transduce the electromagnetic energy to biomechanical signals. We have shown that a significant amount of electromagnetic energy can be efficiently deposited on a carefully engineered mechanical nanoresonator. This is the first, yet crucial step in designing a wireless-to-bio link. Interesting research questions can be formulated on how to use this efficient energy channel to transfer information to a nanoscale device and ultimately a biological organism. Of course a significant theoretical and experimental research is necessary in order to materialize such devices.

Bibliography

- [Ada91] RK Adair. Constraints on biological effects of weak extremely-low-frequency electromagnetic fields. *Physical Review A*, 43(2):1039–1048, 1991.
- [Ada02] RK Adair. Vibrational resonances in biological systems at microwave frequencies. *Biophys J*, 82(3):1147–52, Mar 2002.
- [AFR⁺11] E Alphandéry, S Faure, L Raison, E Duguet, PA Howse, and DA Bazylinski. Heat production by bacterial magnetosomes exposed to an oscillating magnetic field. *The Journal of Physical Chemistry C*, 115(1):18–22, 2011.
- [Ano] WiTricity Corp.
<http://www.witricity.com/pages/technology.html>.
- [BAZ⁺01] E Del Barco, J Asenjo, XX Zhang, R Pieczynski, A Julia, J Tejada, RF Ziolo, D Fiorani, and AM Testa. Free rotation of magnetic nanoparticles in a solid matrix. *Chemistry of materials*, 13(5):1487–1490, 2001.
- [Ben73] C Bennett. Logical reversibility of computation. *IBM journal of Research and Development*, 17(6):525–536, Jan 1973.
- [Ber97] M Berridge. The am and fm of calcium signalling. *Nature*, Jan 1997.
- [Bla75] R Blakemore. Magnetotactic bacteria. *Science*, 190(4212):377–379, 1975.

-
- [BPS⁺08] M Buettner, R Prasad, A Sample, D Yeager, B Greenstein, JR Smith, and D Wetherall. Rfid sensor networks with the intel wisp. pages 393–394, 2008.
- [BW54] JM Blatt and VF Weisskopf. Theoretical nuclear physics. page 864, Jan 1954.
- [Che08] C Chen. Remote control of living cells. *Nature nanotechnology*, Jan 2008.
- [Cif12] M Cifra. Electrodynamic eigenmodes in cellular morphology. *BioSystems*, 109(3):356–66, Sep 2012.
- [CK09] R Cohen and B Kapchits. An optimal wake-up scheduling algorithm for minimizing energy consumption while limiting maximum delay in a mesh sensor network. *Networking, IEEE/ACM Transactions on*, 17(2):570–581, Apr 2009.
- [CM02] A Chaubey and BD Malhotra. Mediated biosensors. *Biosens Bioelectron*, 17(6-7):441–456, Jan 2002.
- [CNB⁺07] J Hyun Choi, FT Nguyen, PW Barone, DA Heller, AE Moll, D Patel, SA Boppart, and MS Strano. Multimodal biomedical imaging with asymmetric single-walled carbon nanotube/iron oxide nanoparticle complexes. *Nano Lett.*, 7(4):861–7, Apr 2007.
- [CW32] JD Cockcroft and ETS Walton. Experiments with high velocity positive ions. (i) further developments in the method of obtaining high velocity positive ions. *Proceedings of the Royal Society of London. Series A*, 136(830):619–630, 1932.
- [CZB⁺10] LM Correia, D Zeller, O Blume, D Ferling, Y Jading, I Gó anddor, G Auer, and L Van Der Perre. Challenges and enabling technologies for energy aware mobile radio networks. *Communications Magazine, IEEE*, 48(11):66–72, Nov 2010.
- [DKPS10] MI Dykman, M Khasin, J Portman, and SW Shaw. Spectrum of an oscillator with jumping frequency and the interference of partial susceptibilities. *Phys. Rev. Lett.*, 105(23):230601, Jan 2010.

- [Dob08] J Dobson. Remote control of cellular behaviour with magnetic nanoparticles. *Nature nanotechnology*, Jan 2008.
- [DPM⁺09] CL Degen, M Poggio, HJ Mamin, CT Rettner, and D Rugar. Nanoscale magnetic resonance imaging. *P Natl Acad Sci Usa*, 106(5):1313–1317, Jan 2009.
- [Dru00] D Drubach. The brain explained. page 168, Jan 2000.
- [EHK⁺07] V Ermolov, M Heino, A Karkkainen, R Lehtiniemi, N Nefedov, P Pasanen, Z Radivojevic, M Rouvala, T Ryhanen, E Seppala, and M Uusitalo. Significance of nanotechnology for future wireless devices and communications. *Personal, Indoor and Mobile Radio Communications, 2007. PIMRC 2007. IEEE 18th International Symposium on*, pages 1 – 5, 2007.
- [EPC08] EPCglobal Standards and Technology, <http://www.epcglobalinc.org/standards>. 2008.
- [FK07] T Falas and H Kashani. Two-dimensional bar-code decoding with camera-equipped mobile phones. pages 597 –600, Mar 2007.
- [För48] T Förster. Zwischenmolekulare energiewanderung und fluoreszenz. *Annalen der Physik*, Jan 1948.
- [GFM95] M Glogauer, J Ferrier, and C A McCulloch. Magnetic fields applied to collagen-coated ferric oxide beads induce stretch-activated ca^{2+} flux in fibroblasts. *Am J Physiol*, 269(5 Pt 1):C1093–104, Nov 1995.
- [HCK⁺11] D Havelka, M Cifra, O Kučera, J Pokorný, and J Vrba. High-frequency electric field and radiation characteristics of cellular microtubule network. *J Theor Biol*, 286(1):31–40, Oct 2011.
- [HCW⁺12] X Hu, P Cebe, AS Weiss, F Omenetto, and DL Kaplan. Protein-based composite materials. *Materials Today*, 15(5):208–215, May 2012.
- [HDMZ06] R Hergt, S Dutz, R Müller, and M Zeisberger. Magnetic particle hyperthermia: nanoparticle magnetism and materials development for cancer therapy. *Journal of Physics: Condensed Matter*, 18:S2919, 2006.

- [HDZ⁺10] H Huang, S Delikanli, H Zeng, DM Ferkey, and A Pralle. Remote control of ion channels and neurons through magnetic-field heating of nanoparticles. *Nature Nanotechnology*, 5(8):602–606, Jan 2010.
- [HH88] J Howard and A J Hudspeth. Compliance of the hair bundle associated with gating of mechanoelectrical transduction channels in the bullfrog’s saccular hair cell. *Neuron*, 1(3):189–99, May 1988.
- [HHD05] S Hughes, AJ El Haj, and J Dobson. Magnetic micro- and nanoparticle mediated activation of mechanosensitive ion channels. *Medical engineering & physics*, 27(9):754–62, Nov 2005.
- [HKJS07] RE Hamam, A Karalis, JD Joannopoulos, and M Soljačić. Coupled-mode theory for general free-space resonant scattering of waves. *Phys. Rev. A*, 75(5):53801, 2007.
- [HMDH08] S Hughes, S McBain, J Dobson, and AJ El Haj. Selective activation of mechanosensitive ion channels using magnetic particles. *J R Soc Interface*, 5(25):855–63, Aug 2008.
- [HTC] HTC dream (T-mobile g1), <http://www.htc.com/www/product/dream/overview.html>.
- [Jac67] JD Jackson. *Classical electrodynamics*. 1967.
- [JBN11a] H Javaheri, B Barbiellini, and G Noubir. Efficient magnetic torque transduction in biological environments using tunable nanomechanical resonators. *Proceedings of the IEEE EMBC 2011*, 2011.
- [JBN11b] H Javaheri, B Barbiellini, and G Noubir. Efficient magnetic torque transduction in biological environments using tunable nanomechanical resonators. *Conf Proc IEEE Eng Med Biol Soc*, 2011:1863–6, Jan 2011.
- [JBN11c] H Javaheri, B Barbiellini, and G Noubir. On the energy transfer performance of mechanical nanoresonators coupled with electromagnetic fields. *arXiv*, cond-mat.mes-hall, Aug 2011. 4 Pages, 1 Figure.

- [JBN12] H Javaheri, B Barbiellini, and G Noubir. On the energy transfer performance of mechanical nanoresonators coupled with electromagnetic fields. *Nanoscale Res Lett*, 7(1):572, Oct 2012.
- [JN10] H Javaheri and G Noubir. ipoint: A platform-independent passive information kiosk for cell phones. *Sensor Mesh and Ad Hoc Communications and Networks (SECON), 2010 7th Annual IEEE Communications Society Conference on*, pages 1 – 9, 2010.
- [JNN09] H Javaheri, G Noubir, and S Noubir. Rf control of biological systems: Applications to wireless sensor networks. *Nano-Net*, Jan 2009.
- [JSvO⁺09] XJA Janssen, AJ Schellekens, K van Ommering, LJ van IJzen-doorn, and MW J Prins. Controlled torque on superparamagnetic beads for functional biosensors. *Biosens Bioelectron*, 24(7):1937–1941, Jan 2009.
- [JWGZ07] K Jensen, J Weldon, H Garcia, and A Zettl. Nanotube radio. *Nano letters*, 7(11):3508–3511, Jan 2007.
- [Kir92] JL Kirschvink. Comment on ”constraints on biological effects of weak extremely-low-frequency electromagnetic fields”. *Physical Review A*, Jan 1992.
- [KJS08] A Karalis, JD Joannopoulos, and M Soljacic. Efficient wireless non-radiative mid-range energy transfer. *Annals of Physics*, 323(1):34–48, 2008.
- [KK95] A Kobayashi and JL Kirschvink. Magnetoreception and electromagnetic field effects: sensory perception of the geomagnetic field in animals and humans. *ACS Advances in Chemistry Series*, 250:367–394, 1995.
- [KKKDRK92] JL Kirschvink, A Kobayashi-Kirschvink, JC Diaz-Ricci, and SJ Kirschvink. Magnetite in human tissues: a mechanism for the biological effects of weak elf magnetic fields. *Bioelectromagnetics*, Suppl 1:101–13, Jan 1992.
- [KKM⁺07] A Kurs, A Karalis, R Moffatt, JD Joannopoulos, P Fisher, and M Soljacic. Wireless power transfer via strongly coupled magnetic resonances. *Science*, 317(5834):83, 2007.

- [KRU⁺09] DH Kim, EA Rozhkova, IV Ulasov, SD Bader, T Rajh, MS Lesniak, and V Novosad. Biofunctionalized magnetic-vortex microdiscs for targeted cancer-cell destruction. *Nature Materials*, 2009.
- [KWW10] JL Kirschvink, M Winklhofer, and MM Walker. Biophysics of magnetic orientation: strengthening the interface between theory and experimental design. *J R Soc Interface*, 7:S179–S191, Jan 2010.
- [LMF08] T Le, K Mayaram, and T Fiez. Efficient far-field radio frequency energy harvesting for passively powered sensor networks. *Solid-State Circuits, IEEE Journal of*, 43(5):1287–1302, May 2008.
- [LOH⁺10] I Lahiri, S Oh, JY Hwang, S Cho, Y Sun, R Banerjee, and W Choi. High capacity and excellent stability of lithium ion battery anode using interface-controlled binder-free multiwall carbon nanotubes grown on copper. *ACS Nano*, 4(6):3440–3446, 2010.
- [Mal74] R Malcolm. A mechanism by which the hair cells of the inner ear transduce mechanical energy into a modulated train of action potentials. *The Journal of General Physiology*, 63(6):757, 1974.
- [MAR⁺00] CJ Meyer, FJ Alenghat, P Rim, JH Fong, B Fabry, and DE Ingber. Mechanical control of cyclic amp signalling and gene transcription through integrins. *Nat Cell Biol*, 2(9):666–8, Sep 2000.
- [Mei01] L Meirovitch. *Fundamentals of Vibrations*. 2001.
- [MM02] JO McSpadden and JC Mankins. Space solar power programs and microwave wireless power transmission technology. *Microwave Magazine, IEEE*, 3(4):46–57, Dec 2002.
- [MW09] AR Muxworthy and W Williams. Critical superparamagnetic/single-domain grain sizes in interacting magnetite particles: implications for magnetosome crystals. *J R Soc Interface*, 6(41):1207–12, Dec 2009.
- [MWH⁺09] A Mohan, G Woo, S Hiura, Q Smithwick, and R Raskar. Bokode: imperceptible visual tags for camera based interaction from a distance. *ACM Trans. Graph.*, 28(3):98:1–98:8, 2009.

- [nfc] The Near Field Communication Forum,
<http://www.nfc-forum.org/>.
- [NRB08] PC Nelson, M Radosavljević, and S Bromberg. Biological physics: energy, information, life. page 630, Jan 2008.
- [NSK⁺08] T Nakano, T Suda, T Koujin, T Haraguchi, and Y Hiraoka. Molecular communication through gap junction channels. *Transactions on Computational Systems Biology X*, Dec 2008.
- [NSM⁺05] T Nakano, T Suda, M Moore, R Egashira, A Enomoto, and K Arima. Molecular communication for nanomachines using intercellular calcium signaling. *Nanotechnology, 2005. 5th IEEE Conference on*, pages 478 – 481 vol. 2, 2005.
- [PF95] EM Phizicky and S Fields. Protein-protein interactions: methods for detection and analysis. *Microbiol Rev*, 59(1):94–123, Mar 1995.
- [POM10] A Poon, S O’Driscoll, and T Meng. Optimal frequency for wireless power transmission into dispersive tissue. *Antennas and Propagation, IEEE Transactions on*, 58(5):1739 – 1750, 2010.
- [Poo09] ASY Poon. Miniaturization of implantable wireless power receiver. *Conf Proc IEEE Eng Med Biol Soc*, 2009:3217–20, Jan 2009.
- [pow] PowerCast corporation,
<http://www.powercastco.com/technology/powerharvester-receivers>.
- [PS08] JG Proakis and M Salehi. *Digital Communications*. 2008.
- [Rab02] J Rabaey. Wireless beyond the third generation-facing the energy challenge. *Low Power Electronics and Design*, Jan 2002.
- [Ric] SO Rice. *Mathematical Analysis of Random Noise*.
- [RL12] AK RamRakhyani and G Lazzi. On the design of efficient multi-coil telemetry system for biomedical implants. *Biomedical Circuits and Systems, IEEE Transactions on*, PP(99):1, 2012.

- [RSPS02] V Raghunathan, C Schurgers, Sung Park, and MB Srivastava. Energy-aware wireless microsensor networks. *Signal Processing Magazine, IEEE*, 19(2):40–50, Mar 2002.
- [Saz06] VA Sazonova. A tunable carbon nanotube resonator. 2006.
- [SCWB08] D Soloveichik, M Cook, E Winfree, and J Bruck. Computation with finite stochastic chemical reaction networks. *Natural Computing: an international journal*, 7(4), Dec 2008.
- [SEK08] RP Shetty, D Endy, and TF Knight. Engineering biobrick vectors from biobrick parts. *J Biol Eng*, 2:5, Jan 2008.
- [Sid09] JA Sidles. Spin microscopy’s heritage, achievements, and prospects. *P Natl Acad Sci Usa*, 106(8):2477–8, Feb 2009.
- [SMS⁺01] B Stipe, H Mamin, T Stowe, T Kenny, and D Rugar. Magnetic dissipation and fluctuations in individual nanomagnets measured by ultrasensitive cantilever magnetometry. *Phys. Rev. Lett.*, 86(13):2874–2877, Mar 2001.
- [SR02] RC Shah and JM Rabaey. Energy aware routing for low energy ad hoc sensor networks. volume 1, pages 350 – 355 vol.1, Mar 2002.
- [SRS03] C Schurgers, V Raghunathan, and MB Srivastava. Power management for energy-aware communication systems. *ACM Trans. Embed. Comput. Syst.*, 2(3):431–447, 2003.
- [SYF⁺08] B Samanta, H Yan, N O Fischer, J Shi, DJ Jerry, and VM Rotello. Protein-passivated fe₃o₄ nanoparticles: low toxicity and rapid heating for thermal therapy. *J. Mater. Chem.*, 18(11):1204, Jan 2008.
- [SYP⁺08] AP Sample, DJ Yeager, PS Powledge, AV Mamishev, and JR Smith. Design of an rfid-based battery-free programmable sensing platform. *Instrumentation and Measurement, IEEE Transactions on*, 57(11):2608–2615, Nov 2008.
- [TKM72] H Takata, O Kogure, and K Murase. Matrix-addressed liquid crystal displays. volume 18, page 72, 1972.

- [TKT⁺12] K Tanaka, M Kenichiro, M Takahashi, T Ishii, and S Sasaki. Development of bread board model for microwave power transmission experiment from space to ground using small scientific satellite. pages 191 –194, May 2012.
- [VRT08] HJ Visser, ACF Reniers, and JAC Theeuwes. Ambient rf energy scavenging: Gsm and wlan power density measurements. pages 721 –724, Oct 2008.
- [Wan05] J Wang. Carbon-nanotube based electrochemical biosensors: a review. *Electroanalysis*, Jan 2005.
- [Wei05] R Weinstein. Rfid: a technical overview and its application to the enterprise. *IT Professional*, 7(3):27 – 33, May 2005.
- [WK10] M Winklhofer and JL Kirschvink. A quantitative assessment of torque-transducer models for magnetoreception. *J R Soc Interface*, 7:S273–S289, Jan 2010.
- [WKK⁺04] BP Weiss, SS Kim, JL Kirschvink, RE Kopp, M Sankaran, A Kobayashi, and A Komeili. Magnetic tests for magnetosome chains in martian meteorite alh84001. *P Natl Acad Sci Usa*, 101(22):8281–8284, Jan 2004.
- [WR08] TM Wendt and LM Reindl. Wake-up methods to extend battery life time of wireless sensor nodes. pages 1407 –1412, May 2008.
- [Yag86] A Yaghjian. An overview of near-field antenna measurements. *IEEE Transactions on Antennas and Propagation*, Jan 1986.
- [YC92] T-W Yoo and K Chang. Theoretical and experimental development of 10 and 35 ghz rectennas. *Microwave Theory and Techniques, IEEE Transactions on*, 40(6):1259 –1266, Jun 1992.
- [ZSB⁺06] K Zahradka, D Slade, A Bailone, S Sommer, D Averbeck, M Petranovic, AB Lindner, and M Radman. Reassembly of shattered chromosomes in deinococcus radiodurans. *Nature*, 443(7111):569–573, Jan 2006.